Engineering Applications of Computational Fluid Mechanics

ISSN: (Print) (Online) Journal homepage: https://www.tandfonline.com/loi/tcfm20

Delft3D model-based estuarine suspended sediment budget with morphodynamic changes of the channel-shoal complex in a mega fluvial-tidal delta

Jie Wang, Ao Chu, Zhijun Dai & Jaap Nienhuis

To cite this article: Jie Wang, Ao Chu, Zhijun Dai & Jaap Nienhuis (2024) Delft3D model-based estuarine suspended sediment budget with morphodynamic changes of the channel-shoal complex in a mega fluvial-tidal delta, Engineering Applications of Computational Fluid Mechanics, 18:1, 2300763, DOI: 10.1080/19942060.2023.2300763

To link to this article: https://doi.org/10.1080/19942060.2023.2300763

ENGINEERING APPLICATIONS OF COMPUTATIONAL FLUID MECHANICS
2024, VOL. 18, NO. 1, 2300763
https://doi.org/10.1080/19942060.2023.2300763

Delft3D model-based estuarine suspended sediment budget with morphodynamic changes of the channel-shoal complex in a mega fluvial-tidal delta

Jie Wang[a,c], Ao Chu[d], Zhijun Dai[a,b] and Jaap Nienhuis[c]

[a]State Key Laboratory of Estuarine and Coastal Research, East China Normal University, Shanghai, People's Republic of China; [b]Laboratory for Marine Geology, Qingdao National Laboratory for Marine Science and Technology, Qingdao, People's Republic of China; [c]Department of Physical Geography, Faculty of Geosciences, Utrecht University, Utrecht, the Netherlands; [d]Institute of Water Science and Technology, Hohai University, Nanjing, People's Republic of China

ABSTRACT

Reduced riverine sediment supply and sea-level rise (SLR) threaten land building and ecosystem in deltas. However, the sediment-morphodynamic processes in a channel-shoal complex are not well understood. Here, based on bathymetry and the Delft3D model, geomorphic changes and suspended sediment budgets in the South Passage, Nanhui and Jiuduansha Shoal in the mega-Changjiang Delta were examined. Results reveal that with riverine suspended sediment concentration (SSC) decreased by 75%, the net sediment deposition rate was reduced from 4.20 cm/yr in 1979–1990 to 3.21 cm/yr in 1990–2003, and further declined to 2.21 cm/yr in 2003–2013 and 0.40 cm/yr in 2013–2020. Severe erosion occurred along the upper South Passage and extended toward the mouth bar. Strong accretions accumulated in the Nanhui and Jiuduansha Shoal. After river SSC declined from 0.53 kg/m^3 to 0.35 kg/m^3, 0.16 kg/m^3, and 0.12 kg/m^3, net suspended sediment deposition was lowered by 3.13%, 7.35% and 8.67%, respectively. Moreover, SLR of 5 cm, 15 cm, 25 cm, and 50 cm resulted in a further 1.11%, 4.18%, 4.16%, and 14.79% reduction in sediment trapping efficiency. Our findings highlight the strong likelihood that reduced river sediment input, SLRs and intensified anthropogenic effects will exacerbate sediment deficit and erosion in mega fluvial-tidal deltas.

ARTICLE HISTORY
Received 14 November 2023
Accepted 26 December 2023

KEYWORDS
Channel-shoal morphodynamics; suspended sediment budget; sea-level rise; Delft3D model; the Changjiang (Yangtze) Delta

1. Introduction

River sediment supply to fluvial-tidal deltas is crucial for geomorphic stability, ecological services, and resilience to storm surges (Goodbred & Kuehl, 1999; Syvitski et al., 2009). Meanwhile, sediment deposition in deltas is governed not only by river sediment supply but also by marine hydrodynamic conditions, delta channel patterns, and delta front shoals (Allison, 1998; Fagherazzi et al., 2015; Szczuciński et al., 2013). Global climate change and high-intensity human activities have resulted in reduced riverine water and sediment supplies entering deltas since the last century (Blum & Roberts, 2009; Dunn et al., 2019; Tang et al., 2013). Relative sea-level rise (SLR) and local engineering work further heighten the uncertainty of delta sediment sources and sinks (Becker et al., 2020; Ibàñez et al., 1997).

Suspended sediment budgets in mega-deltas in particular are sensitive to shifts in hydrodynamics and topographic conditions. And their abundance or lack thereof will influence land building, marshes creation, and relevant biogeochemical processes (Bianchi & Allison, 2009; Caldwell & Edmonds, 2014; Vasilopoulos et al., 2021). The properties of riverine inputs and spatial–temporal variations in relative dominance between tides and waves can determine deltaic morphodynamic processes (Allison et al., 2017; Goodbred et al., 2003; Nienhuis et al., 2020; Porebski & Steel, 2006). However, the total amount of sediment entering the oceans transported by most of the mega-rivers has declined since the 1950s (Syvitski et al., 2022), which coupled with SLR and anthropogenic disturbances greatly threatens delta growth (Nienhuis et al., 2023; Tessler et al., 2015).

CONTACT Zhijun Dai zjdai@sklec.ecnu.edu.cn State Key Laboratory of Estuarine and Coastal Research, East China Normal University, Shanghai 200241, People's Republic of China

Supplemental data for this article can be accessed online at https://doi.org/10.1080/19942060.2023.2300763.

Therefore, understanding the responses of suspended sediment budgets with morphodynamics in a fluvial-tidal delta to changing external drivers is urgent and challenging, especially for low-lying and densely populated mega-deltas (Raff et al., 2023; Yang et al., 2005).

The constriction of the Hoa Binh Dam led to a 61% reduction in annual sediment discharge during 1960–2010 in the Red River Delta, the suspended sediment budget was subsequently altered to achieve a new equilibrium with reduced sedimentation rates (Vinh et al., 2014). Besides, declined riverine sediment input (over 70%) and frequent sand-mining also triggered significant transfer of sediment source-sink in the Mekong Delta, the net sediment outputs from delta distributary channels increased after severe incisions (Thanh et al., 2019; van Binh et al., 2020). In the Mississippi Delta, owing to dropped sediment supply and construction of flood-prevention levees, tidal wetlands were lost by one-quarter; an additional 10,000–13,500 km^2 area would be inundated by 2100 as sediment deficit (Blum & Roberts, 2009; Edmonds et al., 2023). In the future, sediment inputs will continue to decrease in mega-deltas, with mean and maximum reductions of 38% and 83% in 2077–2099 compared to 1990–2019 (Dunn et al., 2019). Meanwhile, rising sea levels influence suspended sediment exchange between different geomorphic units, and the associated variations in sediment transport, budget and retention determine the vulnerability and adaptation in a deltaic channel and tidal shoals (Cazenave & Cozannet, 2014; Talke & Jay, 2020; van Maanen et al., 2013). Fluvial water discharge and tidal forcing exhibit a nonlinear interaction in delta distributaries, strong tides could stabilize the delta geomorphology due to offsetting the net sediment exports during high flows, accompanied by low rates of channel migration (Hoitink et al., 2017; Iwantoro et al., 2022; Porebski & Steel, 2006). In the Wax Lake Delta, erosion during high river flow was centered on the sand shoals adjacent to the channel, whereas erosion during periods of tidal dominance occurred at channel tips and subaqueous areas; the channel widened by 11% between 1991 and 2009 and tidal shoals migrated downstream (Shaw et al., 2013; Shaw & Mohrig, 2014).

Engineering can greatly affect sediment transport and geomorphologic change in mega-deltas, both in the short and long term (Ericson et al., 2006; He et al., 2020; Woodroffe & Murray-Wallace, 2012). The Oosterschelde project of the Dutch Delta project was constructed in 1987 and caused a 30% reduction in the tidal prism. Tidal shoals and salt marshes started to erode; and dam-induced sediment decline, sand mining, and land reclamations in the Rhine-Meuse Delta further triggered the sediment budget turned to negative state (Cox et al., 2021; Louters et al., 1998; van der Spek & Elias, 2021). In the LingDing Bay of the Pearl River Delta, land reclamation between 1988 and 2008 contributed to the reduction of tidal shoals (above −2 m) by 180 km^2, while dredging increased the channel (deeper than −10 m) extent by 36 km^2 (Wu et al., 2014).

The Delft3D numerical model is an efficient tool to study the hydro-sediment dynamics and geomorphic responses to changing drivers in deltas, tidal bays, and coastal areas (Caldwell & Edmonds, 2014; Elmilady et al., 2022; Zhang et al., 2018a). With Delft3D, van der Wegen (2013) found that the interaction between tidal forcing and basin geometry significantly influenced geomorphic features in the Western Scheldt Estuary, and formed a distinct channel-shoal pattern in a few decades. In the San Pablo Bay estuary, California, the model predictions suggested that deeper shoals and reduced river sediment inputs over the next 30 years will lead to a lower Suspended Sediment Concentration (SSC) in the channel, and weaken channel margin deposition (van der Wegen & Jaffe, 2014). Delft3D simulations by Akter et al. (2021) quantified the sediment discharge delivered into the Ganges-Brahmaputra-Meghna Delta by the Ganges and Jamuna rivers to be about 216–1038 × 10^8 t/yr and 80–228 × 10^8 t/yr and proposed the proportions deposited in different parts in the delta. In addition, modeled results also pointed out that tidal currents are the critical agent of SLR-induced change (Elmilady et al., 2022). Despite these studies, the specific differences in suspended sediment budgets between channels and shoals are not well recognized, thus, there is room to increase the understanding of geomorphic change triggered by multiple stresses in a mega fluvial-tidal delta.

The Changjiang (Yangtze) Delta is a typical mega fluvial-tidal delta, influenced by the East Asian monsoon (Figure 1A-B) (Chen et al., 1988; Hori et al., 2002). The subaerial Changjiang Delta is densely populated and low-lying, with an average elevation of 2–4 m. Four bifurcated subaqueous channels (with high navigability) and extensive tidal shoals developed over the past 2,000 years (Figure 1C) (Chen et al., 1999; Liu et al., 2007). Between 1950 and 2020, the mean annual water and suspended sediment discharge at Datong station (the tidal limit) delivered into Changjiang Delta were 8.98 × 10^{11} m^3/yr and 3.51 × 10^8 t/yr, respectively (CWRC, 2022). Since the 1950s, cascading dams (over 50,000) and water-soil conservations in the basin have been implemented (Yang et al., 2005). Thus, annual suspended sediment discharge from the Changjiang River was reduced sharply by more than 70% in the 2010s, especially after the construction of the Three Gorges Dam in 2003, while mean water discharge remained stable (Dai, 2021; Yang et al., 2015).

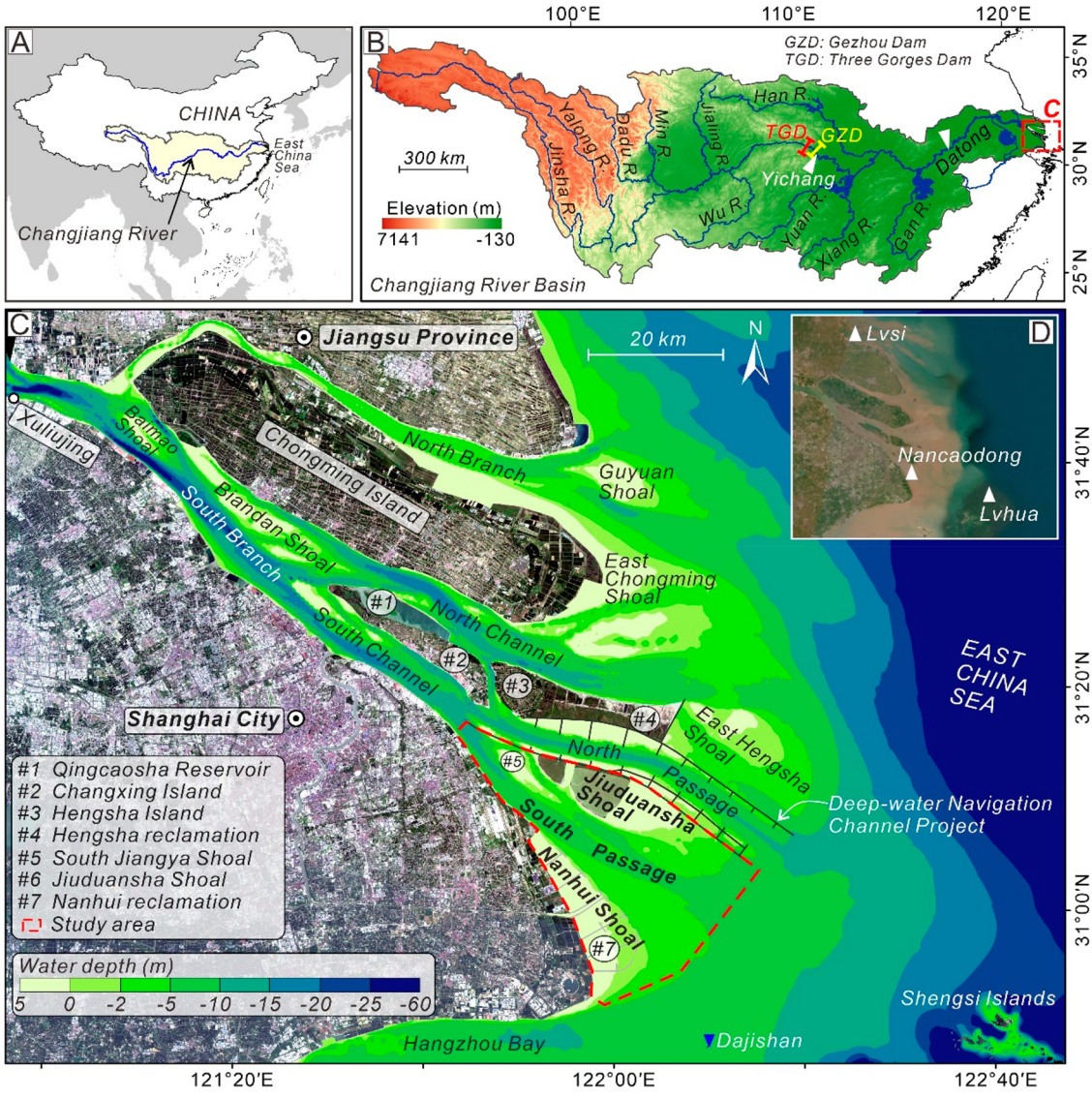

Figure 1. Map of the study area. (A) Location of the Changjiang River in China. (B) Primary distributaries and elevation of the Changjiang River Basin, meanwhile, the Three Gorges Dam, Gezhou Dam and two hydrological stations (Yichang and Datong) were also shown. (C) Three-order bifurcated configuration of the Changjiang Delta with four outlets, the geomorphic complexes of South Passage and bordering Nanhui Shoal and Jiuduansha Shoal is indicated by a red dashed polygon. (D) Three long-term tidal gauging stations around the Changjiang Delta.

As a result, the middle-lower reaches of the Changjiang River and deltaic tidal shoals/flats and landward transport from the subaqueous areas became significant sediment sources rather than sinks (Gao et al., 2018a; Gao et al., 2019; Dai et al., 2014 & Luo et al., 2012; Mei et al., 2021; Wang et al., 2022a). Hence, studies have indicated that the inner delta channels and delta front are eroding, which are further challenged by SLR, extreme hydrologic events, and human activities (Dai et al., 2018b; Luan et al., 2021; Mei et al., 2018; Wang et al., 2013; Wang et al., 2018a and 2023). Nevertheless, the synthesized characteristics of geomorphic changes and suspended sediment budgets between deltaic channels and bordering tidal shoals are less well understood, yet they are under serious threats.

The South Passage is the largest distributary in the Changjiang Delta and carries up to 35% of river water and suspended sediment discharge into the ocean (Figure 1C) (Dai et al., 2015; Yun, 2004). The Nanhui Shoal, the largest marginal tidal shoal, and the Jiuduansha Shoal, the largest vegetated uninhabited tidal shoal, develop on either side of the South Passage (Figure 1C) (Chen et al., 1988). Therefore, the South Passage and the adjacent Nanhui Shoal and Jiuduansha Shoal constitute a typical deltaic channel-shoal geomorphic complex in the Changjiang Delta, further influenced by the adjacent land reclamation and the Deep-water Navigation Channel Project (Figure 1C) (Li et al., 2010; Luan et al., 2017; Wei et al., 2016 and 2020).

In this study, the primary objectives are: (1) to understand past geomorphic change in the South Passage and the adjacent shoals from 1979 to 2020; (2) to quantify the impact of reduced river sediment inputs on suspended sediment budgets; (3) to project future changes in suspended sediment budget due to SLR. The findings may provide insights into suspended sediment budgets and morphodynamic changes in other mega fluvial-tidal deltas like the Changjiang Delta, China, triggered by upstream sediment reductions, SLR, and engineering.

2. Study area

The Changjiang River is the longest river in Asia and the third largest in the world, originating from the Tibetan Plateau, China, with a length of 6,300 km and a watershed area of 1.80×10^6 km^2 (Figure 1A-B). The Changjiang Delta is a typical mega fluvial-tidal delta, and developed a progradational sedimentary system beginning from 6 kyr BP, the distributary channels bifurcated by multi-mouth bars (Chen et al., 1988; Hori et al., 2002). Approximately 1.16×10^{12} t sediment has accumulated in the delta plain and subaqueous areas since the Holocene (Liu et al., 2007). A deltaic configuration with three bifurcations and four outlets (North Branch, North Channel, North Passage, and South Passage) evolved, accompanied by frequent migration of deep channels and tidal shoals (Figure 1C) (1999; Yun, 2004 & Chen et al., 1979). The channel widens from 5 km at the upstream entrance to 100 km at the outlet (Figure 1C). The Gezhou Dam and Three Gorges Dam were constructed in the basin in 1988 and 2003, respectively (Figure 1B).

A mouth bar develops in the middle reaches of the South Passage, which deepens both upstream and downstream; the maximum turbidity zone also formed because of the intense runoff and tidal mixing and abundant river sediments (Figure 1C) (Chen et al., 1999; Liu et al., 2007). Hydro- and sediment dynamics in the South Passage, Nanhui Shoal, and Jiuduansha Shoal are dominated by energetic runoff and tidal forcings, with distinct seasonal and spatial variations (Chen et al., 1988). Tidal forcing is irregular, and the flood tidal current separately propagates in the Nanhui Shoal towards the upper South Passage and the northern Hangzhou Bay, the ebb current converges here again (Li, 1991). Restricted by topography and bottom friction, tidal current is ebb dominant in the South Passage and rotational further offshore (Chen et al., 1988; Yun, 2004). The mean and maximum tidal ranges within the middle South Passage are 2.67 and 4.62 m, and the duration of flood and ebb tides is 5.6 and 6.6 h (Figure 1C), respectively (Yun, 2004). Waves are predominantly wind waves and strongest during the monsoon, with prevailing directions from the N and NNE (Shen & Li, 2011). Wave height gradually increases from the offshore area to the mouth bar, and the mean and maximum wave heights are 0.8 and 7.0 m at Dajishan station, respectively (Figure 1C) (Yun, 2004).

Overall, there is a horizontal circulation of water and sediment between deep channels and shallow shoals within this geomorphic complex, which favors the growth of tidal shoals (Shen & Li, 2011). Moreover, the supratidal and part intertidal zones of the Nanhui Shoal have been reclaimed since the 1990s to meet the land requirement; the seaward boundary of the latest siltation-promoting project expanded almost to the −2 m contour (Figure 1C) (Wei et al., 2017; Yun, 2004). Although human activities in the Jiuduansha Shoal are few, the construction of the Deep-water Navigation Channel Project with multiple jetties and groins in the North Passage has resulted in dramatic shifts in hydrodynamic conditions around the north Jiuduansha Shoal (Figure 1C) (Dai et al., 2013; Wei et al., 2017; Zhu et al., 2016).

3. Data acquisition and methods

3.1. Data acquisition

A total of four datasets were collected in this study. First, the annual and monthly water discharge, suspended sediment concentration, and discharge at Datong station between 1956 and 2022 were collected from the Changjiang Water Resources Commission, China (Table S1). Second, the hourly water levels were obtained at Lvsi station (1980–2018), Lvhuashan station (1993–2017), and Naocaodong station (2006–2019) around the Changjiang Delta, respectively (Figure 1D; Table S1). The annual mean tidal levels and overall SLR were calculated. Third, Landsat satellite imageries of the Changjiang Delta between 1974 and 2022 were downloaded from the USGS (United States Geological Survey) Archive (Table S1), to illustrate the shoreline expansion, sandbar growth, and human activities. Fourth, a unique high-spatial resolution bathymetric dataset of the South Passage, Nanhui Shoal, and Jiuduansha Shoal was acquired in 1979, 1990, 2003, 2013, and 2020 from the Changjiang Estuary Waterway Administration Bureau (Figure 1D; Table S1). The depth and position of the surveyed points were synchronously recorded by a DGPS (differential global positioning system) device and a shipborne dual-frequency echo sounder, respectively; and the spatial density of measuring points was 30–50 points/km^2 (Dai et al., 2014; Wang et al., 2020).

The Natural Neighbor Interpolation was used to generate digital elevation models (DEMs) of the study areas

based on original digitized sounding points, then analyze the geomorphic erosion-deposition patterns (Sibson, 1981; Wang et al., 2020). All DEMs were projected to the Beijing-1954 geographic coordinate system; the elevations/depths were referenced to the Wusong Datum (the lowest tide level in Changjiang Delta) (Dai et al., 2015). The net geomorphic change during different stages can be figured out by subtracting two subsequent DEM raster layers (Eqs. 1 and 2).

$$\Delta D(x,y,t_1,t_2) = D_2(x,y,t_2) - D_1(x,y,t_1) \quad (1)$$

$$Mean(x,y,t_1,t_2) = \Delta D(x,y,t_1,t_2)/(t_2 - t_1) \quad (2)$$

where $D_1(x,y,t_1)$ and $D(x,y,t_2)$ are the depths at any position (x,y) in times t_1 and t_2, $\Delta D(x,y,t_1,t_2)$ and $Mean(x,y,t_1,t_2)$ are the total and annual variation thickness. The thalweg of the South Passage in 2020 was produced and then the depths along thalweg were extracted. In addition, mean thicknesses of net erosion/deposition within different depths were also calculated to examine the vertical differences of geomorphic changes.

3.2. Model setup and different scenarios

3.2.1. Hydrodynamic and sediment-salt transport model

Here, the process-based Delft3D numerical model coupling hydrodynamics and sediment transports was used, to quantify the variations in suspended sediment budgets in the Changjiang Delta under different scenarios (Caldwell & Edmonds, 2014; Chu et al., 2020). The flow module in the Delft3D numerical model is based on the three-dimensional incompressible Navier-Stokes equations and shallow water assumptions, the orthogonal curvilinear coordinates in the horizontal direction are adopted for the discrete solver of the flow field, and the σ-coordinate system is used in the vertical direction (Eq. 3) (Deltares, 2014).

$$\sigma = \frac{z-\zeta}{d+\zeta} = \frac{z-\zeta}{H} \quad (3)$$

where z is the vertical coordinate, ζ is the free liquid surface, d is the water depth of reference base (m), and H is the total depth (m). The continuity and momentum equations are as follows (Eqs. 4–6):

$$\frac{\partial \zeta}{\partial t} + \frac{1}{\sqrt{G_{\xi\xi}}\sqrt{G_{\eta\eta}}}\frac{\partial\left[(d+\zeta)u\sqrt{G_{\eta\eta}}\right]}{\partial \xi} + \frac{1}{\sqrt{G_{\xi\xi}}\sqrt{G_{\eta\eta}}}\frac{\partial\left[(d+\zeta)u\sqrt{G_{\xi\xi}}\right]}{\partial \eta} + \frac{\partial \omega}{\partial \sigma} = H(q_{in} - q_{out}) \quad (4)$$

$$\frac{\partial u}{\partial t} + \frac{u}{\sqrt{G_{\xi\xi}}}\frac{\partial u}{\partial \xi} + \frac{v}{\sqrt{G_{\eta\eta}}}\frac{\partial u}{\partial \eta} + \frac{\omega}{d+\zeta}\frac{\partial u}{\partial \sigma} + \frac{uv}{\sqrt{G_{\xi\xi}}\sqrt{G_{\eta\eta}}}\frac{\partial\sqrt{G_{\xi\xi}}}{\partial \eta} - \frac{v^2}{\sqrt{G_{\xi\xi}}\sqrt{G_{\eta\eta}}}\frac{\partial\sqrt{G_{\eta\eta}}}{\partial \xi} - fv = -\frac{1}{\rho_0\sqrt{G_{\xi\xi}}}P_\xi + F_\xi + \frac{1}{(d+\zeta)^2}\frac{\partial}{\partial \sigma}\left(\upsilon_V\frac{\partial u}{\partial \sigma}\right) + M_\xi \quad (5)$$

$$\frac{\partial v}{\partial t} + \frac{u}{\sqrt{G_{\xi\xi}}}\frac{\partial v}{\partial \xi} + \frac{v}{\sqrt{G_{\eta\eta}}}\frac{\partial v}{\partial \eta} + \frac{\omega}{d+\zeta}\frac{\partial v}{\partial \sigma} + \frac{uv}{\sqrt{G_{\xi\xi}}\sqrt{G_{\eta\eta}}}\frac{\partial\sqrt{G_{\eta\eta}}}{\partial \xi} - \frac{u^2}{\sqrt{G_{\xi\xi}}\sqrt{G_{\eta\eta}}}\frac{\partial\sqrt{G_{\xi\xi}}}{\partial \eta} - fu = -\frac{1}{\rho_0\sqrt{G_{\eta\eta}}}P_\eta + F_\eta + \frac{1}{(d+\zeta)^2}\frac{\partial}{\partial \sigma}\left(\upsilon_V\frac{\partial v}{\partial \sigma}\right) + M_\eta \quad (6)$$

where ζ is the water level above reference base (m); ξ and η are the coordinates of the horizontal orthogonal curves (m); t is time (s); u, v and ω are the flow velocities in the ξ, η and σ directions (m/s); U and V are the mean flow velocities in the ξ and η directions (m/s), respectively; $\sqrt{G_{\xi\xi}}$ and $\sqrt{G_{\eta\eta}}$ are the conversion coefficients between the curvilinear orthogonal coordinate system and the Cartesian coordinate system; q_{in} and q_{out} are the inflow and outflow per unit volume (m^3), respectively; ρ_0 is the density of water (kg/m^3); f is the Coriolis force parameter (1/s); υ_V is the vertical vortex viscosity coefficient (m^2/s, they are obtained using the k-ϵ turbulence model); P_ξ and P_η are the pressure gradients due to density changes in the directions ξ and η, respectively; F_ξ and F_η are the Reynolds stresses caused by turbulence changes the in the directions ξ and η, respectively; M_ξ and M_η are changes in momentum caused by external driving forces (withdrawal, wave radiation stress, etc.) the in the directions ξ and η, respectively. The advection–diffusion equation for suspended sediment in three dimensions is (Eq. 7) (Deltares, 2014):

$$\frac{\partial c^{(l)}}{\partial t} + \frac{\partial uc^{(l)}}{\partial x} + \frac{\partial vc^{(l)}}{\partial y} + \frac{\partial (w - w_s^{(l)})c^{(l)}}{\partial z} - \frac{\partial}{\partial x}\left(\varepsilon_{s,x}^{(l)}\frac{\partial c^{(l)}}{\partial x}\right) - \frac{\partial}{\partial y}\left(\varepsilon_{s,y}^{(l)}\frac{\partial c^{(l)}}{\partial y}\right) - \frac{\partial}{\partial z}\left(\varepsilon_{s,z}^{(l)}\frac{\partial c^{(l)}}{\partial z}\right) = E_l - D_l \quad (7)$$

where $c^{(l)}$ is the mass concentration of the l component of the sediment (kg/m^3); $\varepsilon_{s,x}^{(l)}$, $\varepsilon_{s,y}^{(l)}$ and $\varepsilon_{s,z}^{(l)}$ are the

eddy diffusion coefficient of sediment (m^2/s), respectively; $w_s^{(l)}$ is the sediment settling velocity (m/s); E_l and D_l are the erosion and siltation fluxes of the l component of the sediment ($kg/m^2/s$), respectively. The salinity of water is solved based on Eq. 8 (Chu, 2019):

$$\begin{aligned}&\frac{\partial[(d+\zeta)S]}{\partial t}+\frac{1}{\sqrt{G_{\xi\xi}}\sqrt{G_{\eta\eta}}}\left[\frac{\partial\left[(d+\zeta)u\sqrt{G_{\eta\eta}}S\right]}{\partial\xi}\right.\\&\left.+\frac{\partial\left[(d+\zeta)v\sqrt{G_{\xi\xi}}S\right]}{\partial\eta}\right]+\frac{\partial(wS)}{\partial\sigma}\\&=\frac{d+\zeta}{\sqrt{G_{\xi\xi}}\sqrt{G_{\eta\eta}}}\times\left\{\frac{\partial}{\partial\xi}\left[D_H\frac{\sqrt{G_{\eta\eta}}}{\sqrt{G_{\xi\xi}}}\frac{\partial S}{\partial\xi}\right]\right.\\&\left.+\frac{\partial}{\partial\eta}\left[D_H\frac{\sqrt{G_{\xi\xi}}}{\sqrt{G_{\eta\eta}}}\frac{\partial S}{\partial\xi}\right]\right\}\\&+\frac{1}{d+\zeta}\frac{\partial}{\partial\sigma}\left[D_V\frac{\partial S}{\partial\sigma}\right]-\lambda_d(d+\zeta)S+c\end{aligned}\tag{8}$$

where D_H and D_V are the turbulent diffusion coefficients in horizontal and vertical directions (m^2/s), respectively; S is the salinity of water (according to the practical salinity scale). Furthermore, the three-dimensional bed shear stress ($\vec{\tau}_{b_{3D}}$) is computed in the Delft3D model as follows (Ep. 9) (Deltares, 2014):

$$\vec{\tau}_{b_{3D}}=\rho_0 g\vec{U}|\vec{U}|/C_{3D}^2\tag{9}$$

where $\vec{U}$ is the magnitude of the horizontal velocity in the first layer above the bottom bed (m/s), and the C_{3D} is the Chézy roughness coefficient in three dimensions ($m^{1/2}/s$).

3.2.2. Model domain and grids

In this paper, the model domain covered the lower reaches of the Changjiang River (from Datong to Xuliujing), the entire Changjiang Delta, Qiantang River-Hangzhou Bay, and extended eastward to approximately −60 m isobath in the East China Sea and Yellow Sea (Figure 2A). The longitudinal and latitudinal dimensions of the whole domain were about 580 and 360 km, respectively, the complex composed of the South Passage, Nanhui Shoal and Jiuduansha Shoal was located in the middle area (Figure 2A).

The domain decomposition technique was employed to divide the entire study area into three sub-domains, which can be parallelized during model runtime to improve computational efficiency (Figure 2A). They were the Changjiang River sub-domain, the Qiantang River sub-domain, and the Changjiang Delta to adjacent sea sub-domain, which were composed of 1056 × 30, 137 × 6 and 200 × 200 orthogonal curvilinear grids, respectively (Figure 2A) (Chu, 2019). The grid resolution was about 260 m in the upper deltaic channel and varied gradually seaward to 6000 m in the East China Sea. In addition, the σ-coordinate system in the Delft3D model was used for the Changjiang Delta to adjacent sea sub-domain to segment it vertically into 12 layers, (Haney, 1991); portions of the top and bottom sub-layers were lower than that of the middle layers, more details were shown in Chu et al. (2020). The hydrodynamics in the Changjiang River and Qiantang River sub-domains were modeled in two dimensions. Measured high-resolution bathymetric data of study areas was obtained and correlated to generated orthogonal grids. Finally, the multiple jetties-groins of the Deep-water Navigation Channel Project in the North Passage and the siltation-promoting project in the Nanhui Shoal were all defined as overflow weirs in the Delft3D model (Chu, 2019).

3.2.3. Boundary conditions

Two riverine open boundaries were set up at Datong and Luci stations to represent fluvial inputs from the Changjiang River and the Qiantang River, respectively (Figure 2A). At Changjiang River, the daily measured water discharge and related SSC from January 2016 were prescribed for model calibrations and validations. Thereafter, the overall mean water discharge and the phased mean SSC were set to characterize the reduction of upstream sediment inputs. At Qiantang River, the runoff is very low compared to that of the Changjiang River, and its water discharges and SSC were set to fixed values of 1,000 m^3/s and 0.110 kg/m^3 (Chu, 2019).

Suspended sediments in the Changjiang Delta consist mainly of fine-grained silt and clay, while the bottom sediments are more of coarse-grained material such as coarse silt and sand (Chen et al., 1999; Yun, 2004). The amount and properties of riverine input sediments greatly affect the geomorphic changes within the channel-shoal complex. Therefore, a total of three fluvial sediment types were considered in this study based on the properties of upstream input, i.e. the mud (cohesive fine silt and clay), clay (coarse silt), and fine sand, the latter two were non-cohesive with D_{50} of 40 and 200 μm (Chu et al., 2020). Here, the measured sediment concentration at the Datong station was used as the boundary value for the fine fraction. Meanwhile, equilibrium concentration profiles were applied for the two coarse-grained fractions (i.e. coarse silt and fine sand) at the defined boundaries. The salinity at both river open boundaries was set to 0.

Along the seaward open boundaries, a water level was prescribed based on nine primary astronomical tidal constituents: M_2, S_2, N_2, K_2, K_1, O_1, P_1, M_4, and Sa (Figure 2A). Water salinity was set at 34 ppt and SSC at

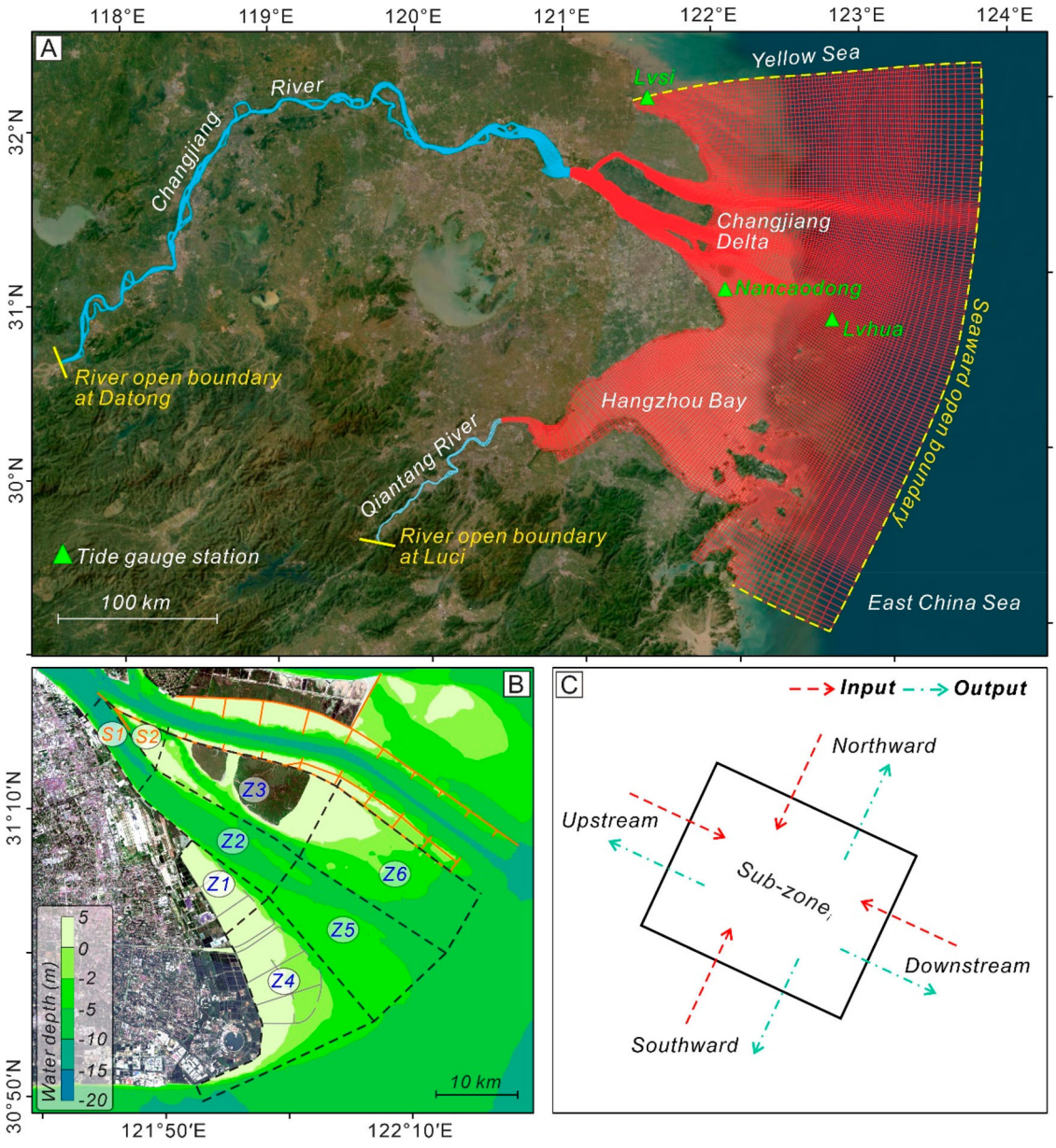

Figure 2. (A) The prescribed domains and grids of the Delft3D model, which were comprised of three sub-regional models, i.e. the Changjiang and Qiantang Rivers (light blue) and the Changjiang Delta (red). The landward river open boundaries (at Datong and Luci, respectively) and seaward open boundaries were indicated here. (B) Based on the geomorphological features and local hydrodynamic conditions, the entire study area was divided into eight sub-zones for the analyses of bathymetric changes and modeled suspended sediment budgets, i.e. S1–S2 and Z1–Z6. (C) A schematic diagram of the calculation of suspended sediment input, output, and net budget for each sub-zone.

0.020 kg/m^3, respectively (Chu, 2019). SLR was implemented by increasing the value of the A_0 constituent.

3.2.4. Model setup and calibration

The coupled hydrodynamic and sediment transport model was realized based on previous studies, which have been calibrated and validated for water level, flow velocity, flow direction, SSC, and water salinity (Chu et al., 2015, 2020). Manning coefficients in the Changjiang River and the deltaic-offshore areas were calibrated to 0.019 and 0.011 s/m$^{1/3}$, respectively; the horizontal viscosity and diffusivity were calibrated to 2 and 1 m^2/s (Chu, 2019; Zhao et al., 2023). In addition, the settling velocity of cohesive sediment related to flocculation was set to 0.25 mm/s, and its specific and dry bed densities were defined to 2650 and 800 kg/m^3, respectively (Chu, 2019; Luan et al., 2017; Zhang et al., 2018a). The time step was set as 60 s to meet the requirements of CFL (Courant–Friedrichs-Lewy number) criteria (Eq. 10); the bathymetry was not updated during the hydrodynamic

modeling (Chu et al., 2020; Deltares, 2014).

$$CFL = 2\Delta t \cdot \sqrt{gh(1/(\Delta x^2 + \Delta y^2))} < 4\sqrt{2} \quad (10)$$

where Δx and Δy are the minimum grid size in the x and y directions, respectively.

3.2.5. Modeling scenario settings

A total of 10 scenarios were set up in the Delft3D model, varying the input SSC at Datong and SLR at the seaward boundary (Table 1). Scenarios C01–C04 follow the past four decades, with a declining SSC from the Changjiang River. The multi-annual mean SSC in each stage was 0.53 kg/m^3 (1965–1988), 0.35 kg/m^3 (1989–2003), 0.16 kg/m^3 (2004–2013) and 0.12 kg/m^3 (2014–2022), i.e. Stage I-IV (Text S1). Figure S1A shows that water discharge entering the mega-Changjiang Delta remained relatively stable between 1956 and 2022, indicating some fluctuations but no obvious global trend of increase or decrease. Therefore, the water discharge from Changjiang River at Datong station was set to a constant value of 28,000 m^3/s in all scenarios, as the stage-by-stage reduction in the riverine-inputted SSC (Figure S1D). Scenarios C06–C08 investigate the effect of future SLR. Considering an SLR rate in the Changjiang Delta of about 5 mm/yr (Text S1), thus the four scenarios were developed to project suspended sediment budgets after 10, 30, 50, and 100 years under rising sea level with a constant rate. Water discharge and SSC were constant at 28,000 m^3/s and 0.12 kg/m^3, with water levels at 5, 15, 25, and 50 cm above modern mean sea level, respectively (Table 1). Scenarios C09–C10 investigate the superimposed effect of a further reduced riverine SSC of 0.060 kg/m^3 in combination with the SLR of 15 and 50 cm, respectively (Table 1).

3.3. Calculation of suspended sediment budget

Each scenario was run for three full semilunar tidal cycles in the Delft3D model (over 45 days), the actual numerical simulation for a single run took about 25 h. Thereafter, modeling results of the last semilunar tidal cycle (coving spring-neap-spring tide, 15 days) were selected to calculate the hydrodynamics and associated suspended sediment budgets (Chu et al., 2020). First, the means of depth-averaged velocities, bed shear stresses and SSCs were worked out; and the differences in hydrodynamic characteristics triggered by lower riverine SSC inputs and SLR can be compared. Here, considering the topographic conditions, the entire channel-shoal geomorphic complex was divided into eight sub-zones (Figure 2B). (1) Sub-zones S1 and S2 were relatively small in spatial extents with significant bathymetric variations, and the latter is adjacent to the jetties-groins of the Deep-water Navigation Channel Project (Figure 2B). (2) Sub-zones Z1 and Z4 occupied the shallower Nanhui Shoal, and were defined as south shoal, and the latest siltation-promoting projects were constructed in intertidal flats (Figure 2B). (3) Sub-zones Z2 and Z5 were located in the South Passage, were defined as the main channel, and were longitudinally bounded by the mouth bar. (4) Sub-zones Z3 and Z6 expanded seaward from the head of Jiuduansha Shoal to the offshore area, defined as the north shoal, bounded by the south training wall of the Deep-water Navigation Channel Project (Figure 2B).

The cross-sections of the sub-zones were then used to calculate the suspended sediment fluxes flowing through them (Chu, 2019). The suspended sediment budget for each sub-zone was derived following Eq. 11 and was based on the input and output fluxes:

$$SSB_i = \sum_{i=1}^{k} input_i - \sum_{i=1}^{k} output_i \quad (11)$$

where SSB_i is the net suspended sediment budget of sub-zone i, $input_i$ and $output_i$ was the suspended sediment flux that input to/output from sub-zone i from/to other neighboring sub-zones, k is the number of sub-zones neighboring. Only the SSB_i of sub-zones Z1–Z6 were determined. The upstream-most sub-zones S1 and S2 were not included to avoid the uncertainties caused by large topographic variations.

Table 1. Riverine inputs (water discharge and SSC) and Sea-level rises (SLRs) for the ten modeled scenarios set up in this study.

Scenario	Water discharge (m^3/s)	SSC (kg/m^3)	SLR (cm)	Describe
C01	28,000	0.53	0	Stage *I* (1956–1985)
C01		0.35		Stage *II* (1986–2003)
C03		0.16		Stage *III* (2004–2013)
C04		0.12		Stage *IV* (2014–2022)
C05	28,000	0.12	5	10 years later
C06			15	30 years later
C07			25	50 years later
C08			50	100 years later
C09	28,000	0.06	15	30 years later with lower SSC
C10			50	100 years later with lower SSC

4. Results

4.1. Observed geomorphic change between 1979 and 2020

Bathymetric data from 1979 shows that the main channel of the South Passage and shoal isobaths were sinuous. The elevation of this geomorphic complex was entirely below 0 m with an overall mean depth of −3.94 m (Figure 3A; Table 2). Bathymetric change between 1979 and 1990 was

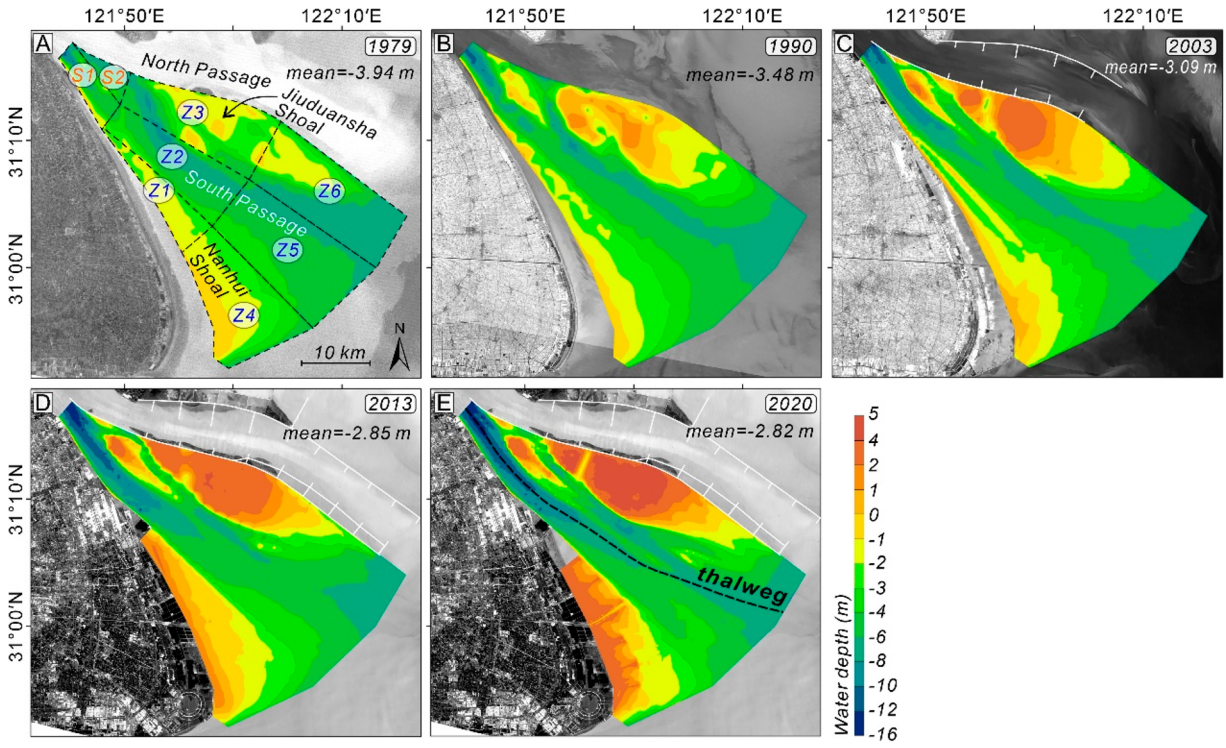

Figure 3. Bathymetries of the geomorphic complexes of South Passage, Nanhui Shoal and Jiuduansha Shoal between 1979 and 2020, the corresponding mean depths were also indicated. Different divided sub-zones and the location of thalweg in 2020 were shown in subgraphs A and E.

Table 2. Mean depth in the entire study area and 8 sub-zones between 1979 and 2020.

	Mean depth (m)				
Extent	1979	1990	2003	2013	2020
Entire	−3.94	−3.48	−3.09	−2.85	−2.82
S1	−4.59	−5.60	−7.41	−8.88	−9.78
S2	−5.64	−2.19	−1.21	−2.03	−1.84
Z1	−1.84	−1.81	−1.50	0.31	1.77
Z2	−5.10	−5.03	−5.33	−5.72	−6.26
Z3	−2.92	−0.96	0.34	1.12	1.45
Z4	−2.07	−2.33	−1.69	−1.09	−0.40
Z5	−5.05	−5.17	−4.87	−4.52	−5.02
Z6	−5.00	−4.23	−3.90	−4.12	−3.85

mainly characterized by deposition in the north and erosion in the south parts. But, deposition dominated and after 4.20 cm/yr of net accretion during Stage I, the mean depth became −3.48 m (Figure 3B and Figure 4A). From 1990 to 2003, the lowering of SSC into the Changjiang Delta caused erosion in the upper South Passage channel and the bordering south Jiuduansha Shoal. Deposition occurred in the Nanhui Shoal and the top of the Jiuduansha Shoal; the overall mean deposition rate was 3.21 cm/yr (Figure 3C and Figure 4B). From 2003 to 2013, after the construction of the Three Gorges Dam, strong erosion along the upper South Passage extended seaward, while growth of the Nanhui Shoal exceeded that of the Jiuduansha Shoal, and the overall net deposition rate declined to 2.21 cm/yr (Figure 3D and Figure 4C). From 2013 to 2020, erosion expanded further downstream, deposition patches were concentrated in the Jiuduansha Shoal and the now-engineered areas in Nanhui Shoal; the net deposition rate dropped rapidly to 0.40 cm/yr (Figure 3E and Figure 4D).

Overall, between 1979 and 2020 the upper South Passage channel experienced erosion, which lowered in magnitude going downstream (Figure 4E). In contrast, after the merger of scattered sandbars and implementation of the Deep-water Navigation Channel Project, the Jiuduansha Shoal showed aggradation and progradation, and in the Nanhui Shoal anthropogenic-induced deposition occurred (Figure 4E). In line with the reduced suspended sediment inputs from the Changjiang River, the net deposition rates of the first three stages were 10.40, 7.95 and 5.48 times that of the last stage; the net deposited sediment were 4.28×10^{11} m^3/yr, 3.27×10^{11} m^3/yr, 2.25×10^{11} m^3/yr and 4.11×10^{10} m^3/yr, respectively. Finally, the distinctive deltaic channel-shoal geomorphic configuration was progressively developed with smoother isobaths (Figures 3 and 4).

The uppermost sub-zone S1 incised between 1979 and 2020, while sub-zone S2 aggraded at a declined rate (Figure 5A-B). The upper Nanhui Shoal and Jiuduansha Shoal (sub-zone Z1 and Z3) accreted, with a mean of 8.89 and 10.69 cm/yr, respectively (Figure 5C and E).

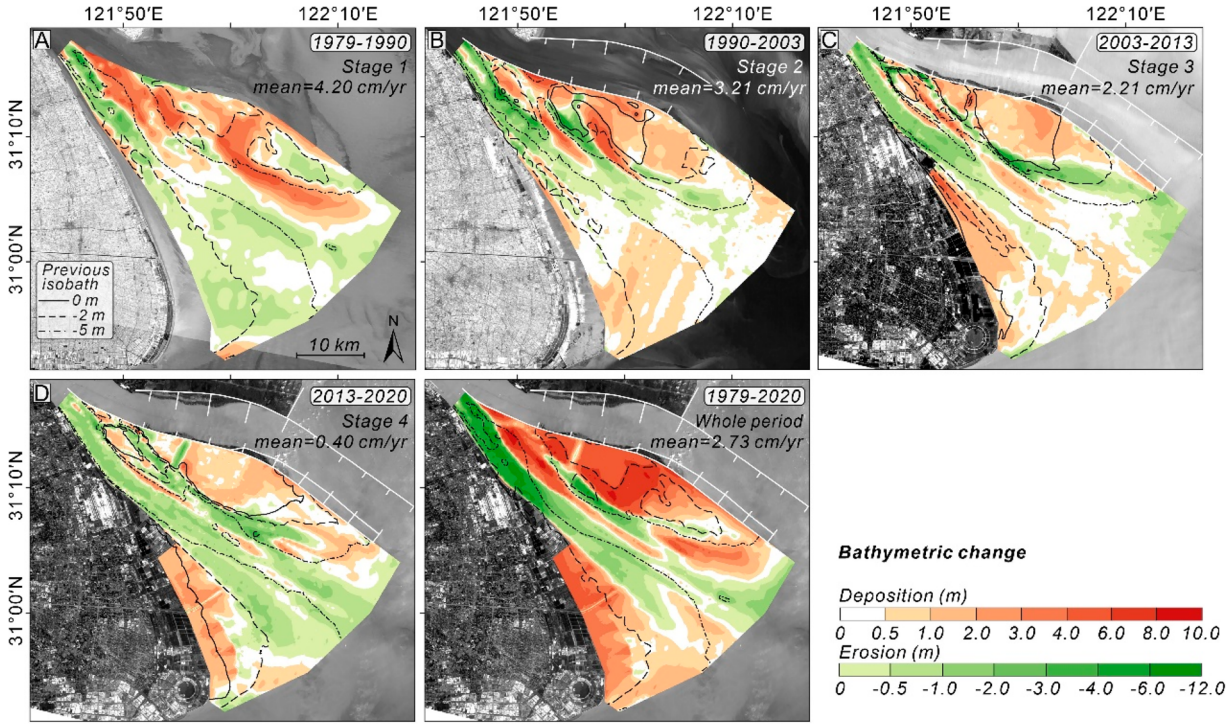

Figure 4. Patterns of geomorphologic change during (A-D) four periods and (E) the whole period between 1979 and 2020. The 0 m, −2 m and −5 m isobaths in all subgraphs correspond to earlier bathymetric data.

However, geomorphic changes in sub-zone Z2 upstream of the mouth bar shifted from 0.59 cm/yr deposition in Stage I to erosion at a later stage (Figure 5D). During Stage I-III, sub-zones Z4 and Z5 showed similar trends from erosion to deposition, but accelerated accretion (17.42 cm/yr) and incision (−7.16 cm/yr) occurred in Stage IV, respectively (Figure 5F-G). Change in sub-zone Z6 in the Jiuduansha Shoal was consistent with the sub-zone S2, both started accreting in Stage IV (Figure 5H).

Depth variations along the thalweg suggested that during Stage I the uppermost South Passage incised, reaching up to −30.55 cm/yr, but there was no overall trend (Figure 5I-J). The incision expanded to the mouth bar in Stage II, leading to a transition of bar pattern from bimodal to unimodal. In Stage III the erosion continued to increase, with more distinct longitudinal heterogeneity (Figure 5I-J). In Stage IV, erosion accelerated and the crest of the mouth bar migrated downstream by 6.5 km (Figure 5I-J). Furthermore, deposition occurred primarily in deeper water in Stage I except for a few fluctuations; in Stage II, the deposition extended to shallower areas (Figure 5K). Geomorphic changes switched in Stage III, when deep channels started to erode and places above −5 water depth, the tidal shoals, accreted. By Stage IV, the threshold depth for accretion moved up to −2 m, after more erosion occurred in areas with middle depth. Shoals still showed net accretion (Figure 5L).

4.2. Suspended sediment budgets under different SSC input scenarios

4.2.1. Modeled hydrodynamics

Modeled depth-averaged flow velocity and bed shear stress in Scenario C04 are illustrated here, as the derived results of Scenarios C01–C04 were consistent (Figure 6A-B). High mean flow velocities with peaks over 1.20 m/s governed the upper South Passage channel, which gradually decreased to the mouth bar at 0.75 m/s, and increased again to 0.85 m/s in the offshore areas (Figure 6A). Meanwhile, from the deep channel to tidal shoals on both sides, velocity reduced and showed a pattern of contours roughly similar to isobaths; the overall mean in this complex was 0.59 m/s (Figure 6A; Table 3). Moreover, the spatial features of bed shear stress were consistent with velocity, with an overall mean of 0.38 N/m^2 in Scenarios C01–C04 (Figure 6B; Table 3).

Modeled SSC in Scenario C04 decreased from 1.00 kg/m^3 in the upper South Passage channel to 0.50 kg/m^3 in the mouth bar, and continued to decline to about 0.35 kg/m^3 in the offshore area (Figure 6C). The SSC exhibited a clear spatial difference in the Jiuduansha Shoal, which was characterized by an aggregation with locally higher value of 0.40–0.50 kg/m^3 at the crest area, it decreased towards the tail (Figure 6C). The overall mean modeled SSC in Scenarios C02–C04 was −0.83%, −1.94% and −2.21% lower than that of Scenarios C01,

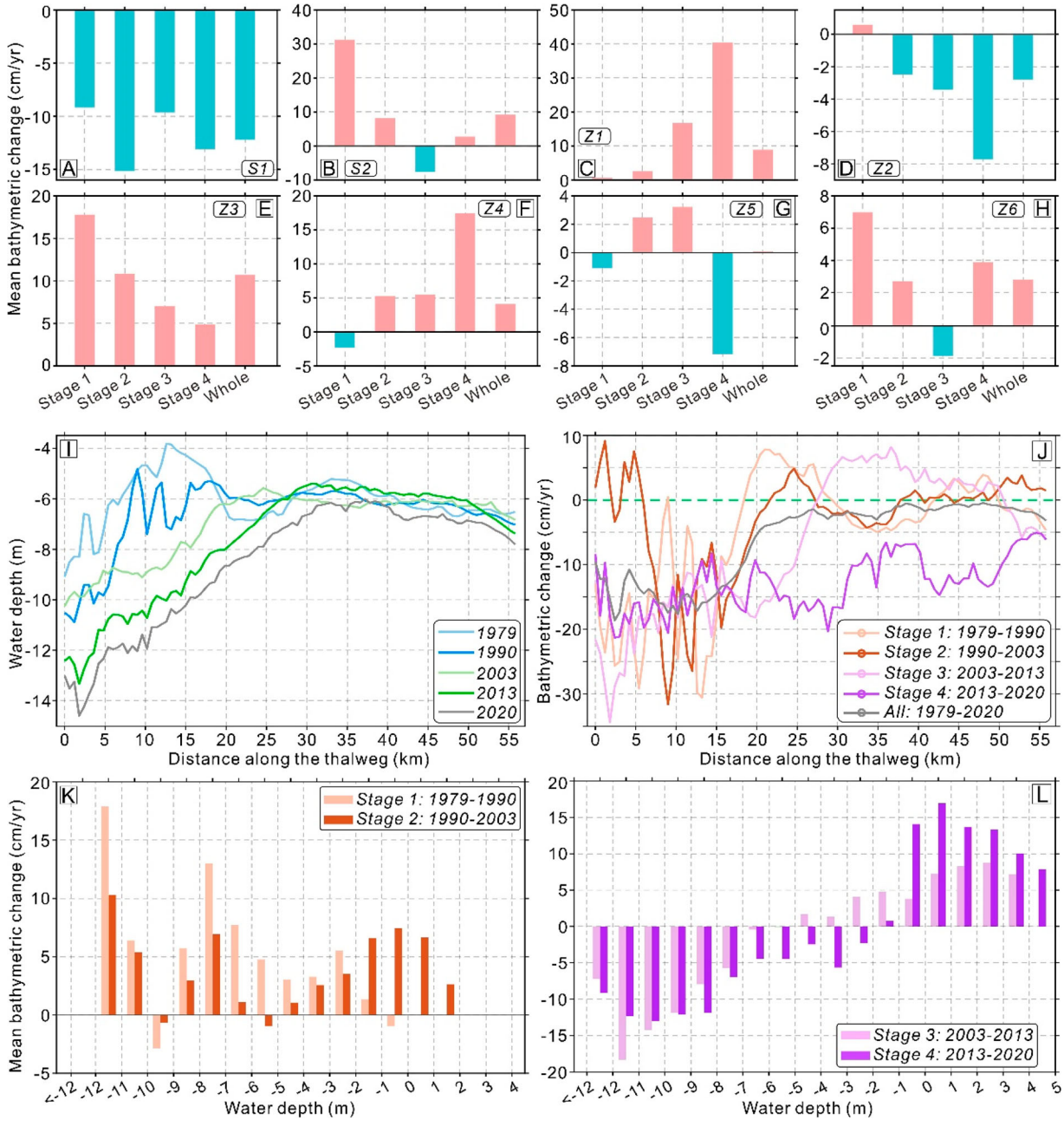

Figure 5. (A-H) Mean bathymetric changes in all divided sub-zones during four stages and the whole period, and the positive/negative values represent geomorphic deposition/erosion, respectively. (I) Water depth and (J) the corresponding changes along the thalweg in the South Passage. (K-L) Mean bathymetric changes in different areas with specific water depths in four stages.

respectively (Table 3). The results from Scenario C01 to Scenario C04 indicated that with the lower SSC input from the Changjiang River, the upstream SSC reduction in the Changjiang Delta was the strongest (exceeding 0.05 kg/m^3), and re-strengthened slightly in the offshore areas after the mouth bar (Figure 6D).

4.2.2. Changes in the suspended sediment budgets

In Scenario C01, there is net deposition in upstream sub-zones Z1–Z3 and sub-zone Z4 in the south Nanhui Shoal, accumulating 2.132×10^6 t, 2.457×10^6 t, 0.042×10^6 t, and 1.075×10^6 t of suspended sediment, respectively (Figure 7A). Subzones Z5–Z6 downstream of the mouth bar experienced net sediment exports of -1.381×10^6 t and -0.179×10^6ï£¡ï£¡ï£¡t, respectively (Figure 7A). The overall trapped net suspended sediment in this geomorphic complex was 4.15×10^6 t (Figure 8A). In particular, the net sediment flux through seaward transects was 0.155×10^6 t, characterized by net output from the main South Passage and input toward the shoals on both sides (Figure 8B; Table 4). In Scenario C02, the net suspended sediment budget in the entire area decreased −3.13%

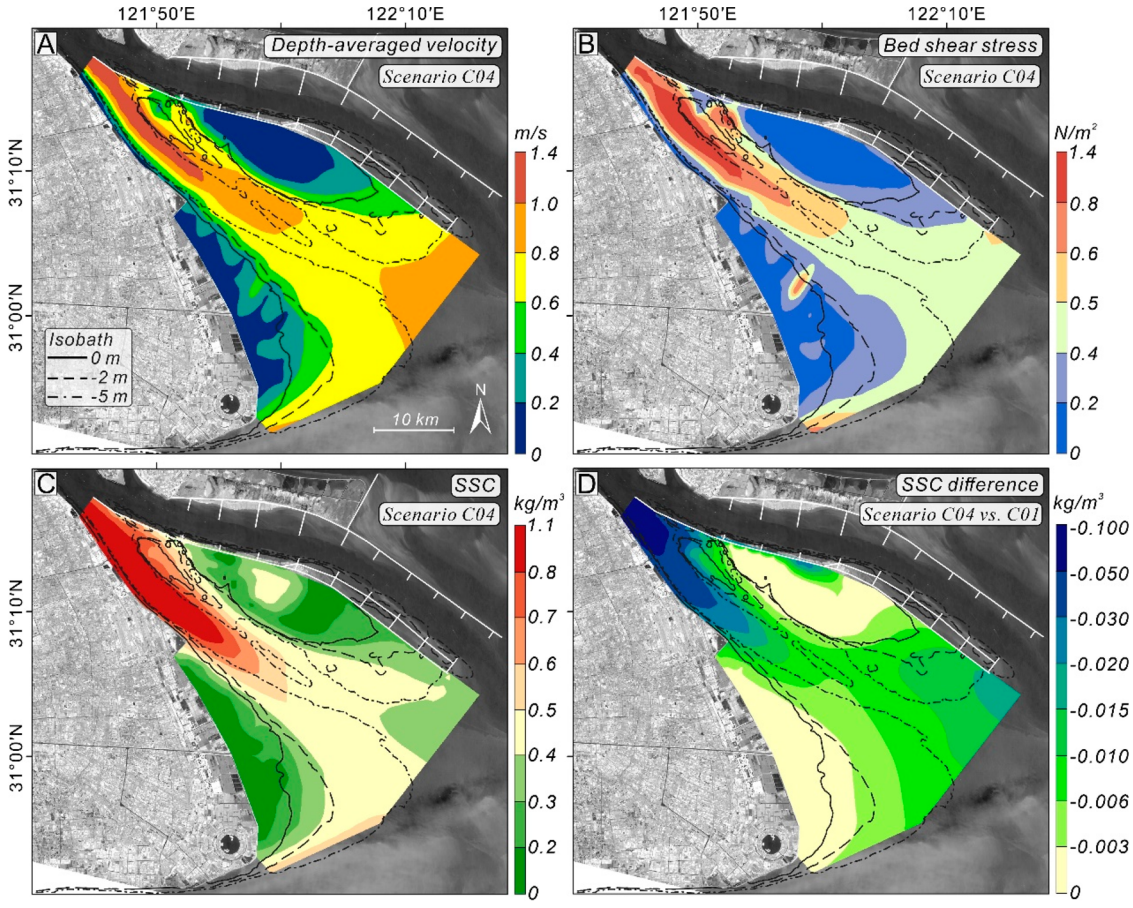

Figure 6. Modeled mean (A) depth-averaged velocity, (B) bed shear stress and (C) suspended sediment concentration in Scenario C04, and (D) the SSC difference between Scenario C04 and C01.

Table 3. Mean values of modeled mean depth-averaged velocity, bed shear stress and SSC and corresponding differences in all scenarios.

	Depth-averaged velocity (m/s)		Bed shear stress (N/m^2)		SSC (kg/m^3)	
Scenario	Mean	Difference *(vs. C04)*	Mean	Difference *(vs. C04)*	Mean	Difference *(vs. C04)*
C01	0.586	/	0.381	/	0.441	/
C02					0.437	−0.83%
C03					0.432	−1.94%
C04					0.431	−2.21%
C05	0.589	0.40%	0.382	0.25%	0.427	−0.95%
C06	0.593	1.20%	0.385	0.80%	0.418	−3.07%
C07	0.598	2.02%	0.387	1.35%	0.413	−4.27%
C08	0.610	4.06%	0.392	2.73%	0.401	−7.00%
C09	0.593	1.20%	0.385	0.80%	0.417	−3.36%
C10	0.610	4.06%	0.392	2.73%	0.400	−7.23%

Table 4. Modeled net suspended sediment flux through the seaward transect (including total, south shoal, main channel and north shoal) in different scenarios.

Scenario	Total (10^6 t)	South shoal (10^6 t)	Main channel (10^6 t)	North shoal (10^6 t)
C01	0.155	3.580	−3.440	0.015
C02	0.126	3.563	−3.435	−0.002
C03	−0.072	3.526	−3.531	−0.067
C04	−0.118	3.512	−3.550	−0.080
C05	0.058	3.481	−3.462	0.039
C06	0.111	3.293	−3.403	0.221
C07	0.598	3.235	−3.194	0.557
C08	1.396	3.281	−2.992	1.107
C09	0.079	3.288	−3.417	0.208
C10	1.350	3.275	−3.019	1.094

Note: Positive and negative values represent the net flux entering and outflowing from the study area, respectively.

to 4.016×10^6 t, but still maintained a similar pattern (Figure 7B and Figure 8A). The net flux along the seaward transects reduced by 17.81% to 0.126×10^6 t, while the outflow to the North Passage increased by 3.79% to 0.916×10^6 t (Figure 8B-C). The sediment budget in net trapping sub-zones, i.e. sub-zones Z1–Z4, were reduced by −0.74%, −1.82%, −18.03%, and −0.59%, respectively (Figure 8D-G). In the sub-zones with an initial net sediment export, i.e. sub-zones Z5–Z6, the export increased by 0.98% and 23.23% (Figure 8H-I).

In Scenarios C03 and C04, following the further reduced SSC inputs from the Changjiang River, the overall net suspended sediment budgets decreased by −7.35% and −8.67% to 3.841×10^6 t and 3.786×10^6 t compared to Scenario C01 (Figure 7C-D and Figure 8A). Suspended

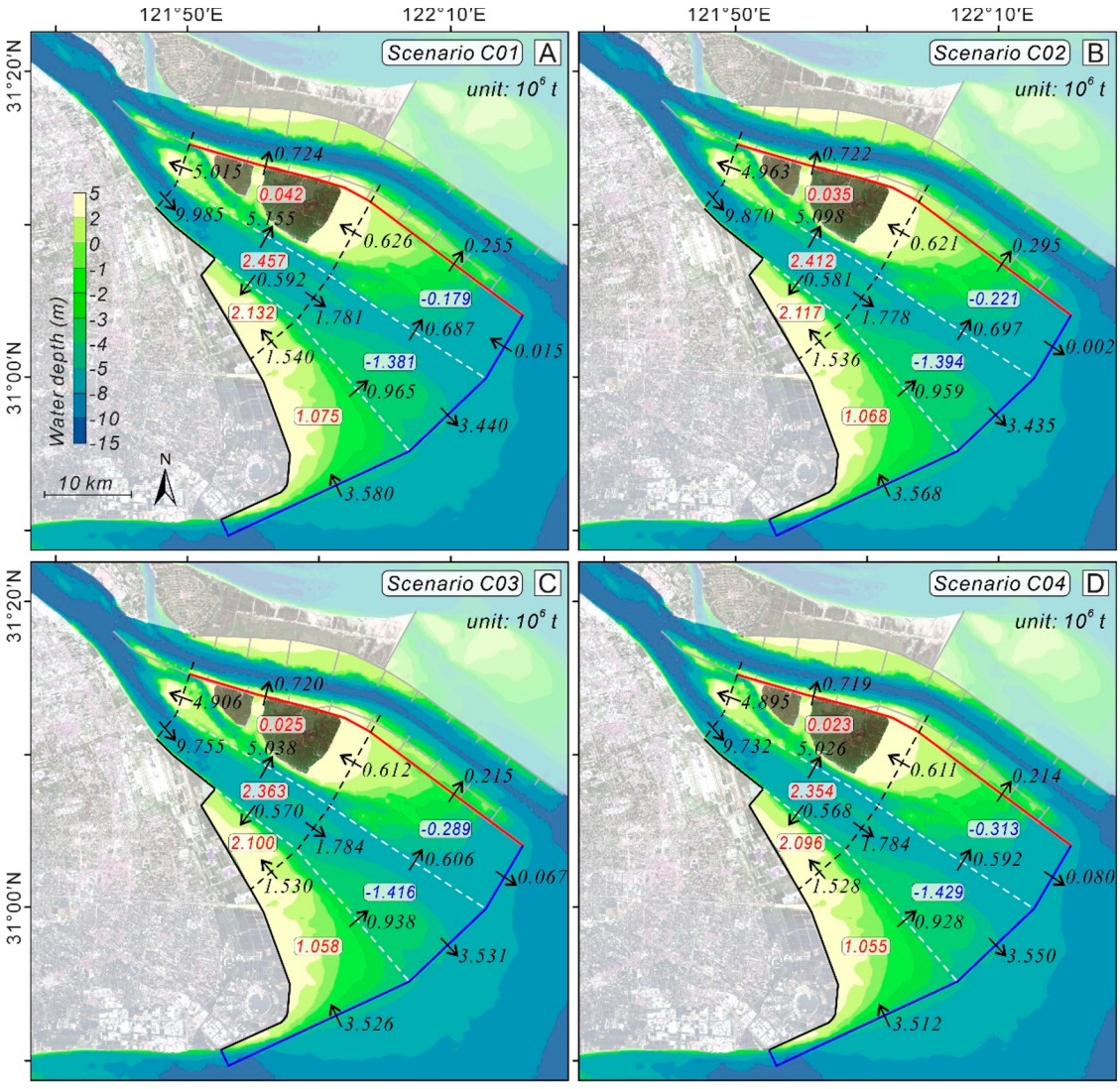

Figure 7. Modeled net suspended sediment fluxes through different transects, and the corresponding sediment budgets within all divided sub-zones in Scenarios C01–C04 (with gradually reduced riverine SSC). Arrows and associated values on the transect between different sub-zones indicate the direction and amount of net suspended sediment transport.

sediment transport along the seaward transects shifted from net landward import (in scenarios C01 and C02) to net export to the offshore areas, as the total flux reached 0.072×10^6 t and 0.118×10^6 t (Figure 7C-D and Figure 8B; Table 4). Export to the North Passage reduced by −6.13% and −6.34% in Scenarios C03–C04 compared to Scenario C01 (Figure 8C). In total, net suspended sediment budgets in sub-zones Z1–Z4 decreased in Scenarios C03–C04 (Figure 8D-G). The net output of suspended sediment from sub-zone Z5 and Z6 further increased by 2.52% and 60.88% in Scenario C03 and 3.47% and 74.23% in Scenario C04 (Figure 8H-I).

In general, with reduced riverine SSC supply, the trapping efficiency of suspended sediment in the accreting sub-zones declined while exports from eroding sub-zones increased (Figures 7 and 8). In particular, in the south shoal, the reduction in net suspended sediment deposition reduced −1.70% from Scenario C01 to Scenario C04. The net export from the north shoal increased by 111.27% (Figure 8J and L). Moreover, the net deposition decreased in the upstream sub-zone Z2 and net output increased in the downstream sub-zone Z5, which resulted in reduced trapping efficiency in the main channel (Figure 8K).

4.3. Suspended sediment budgets under SLR scenarios

4.3.1. Modeled hydrodynamics

Increased mean sea levels by 5, 15, 25, and 100 cm (Scenarios C05–C08), lead to increases in the mean of modeled depth-averaged velocities, by 0.40%, 1.20%, 2.02%,

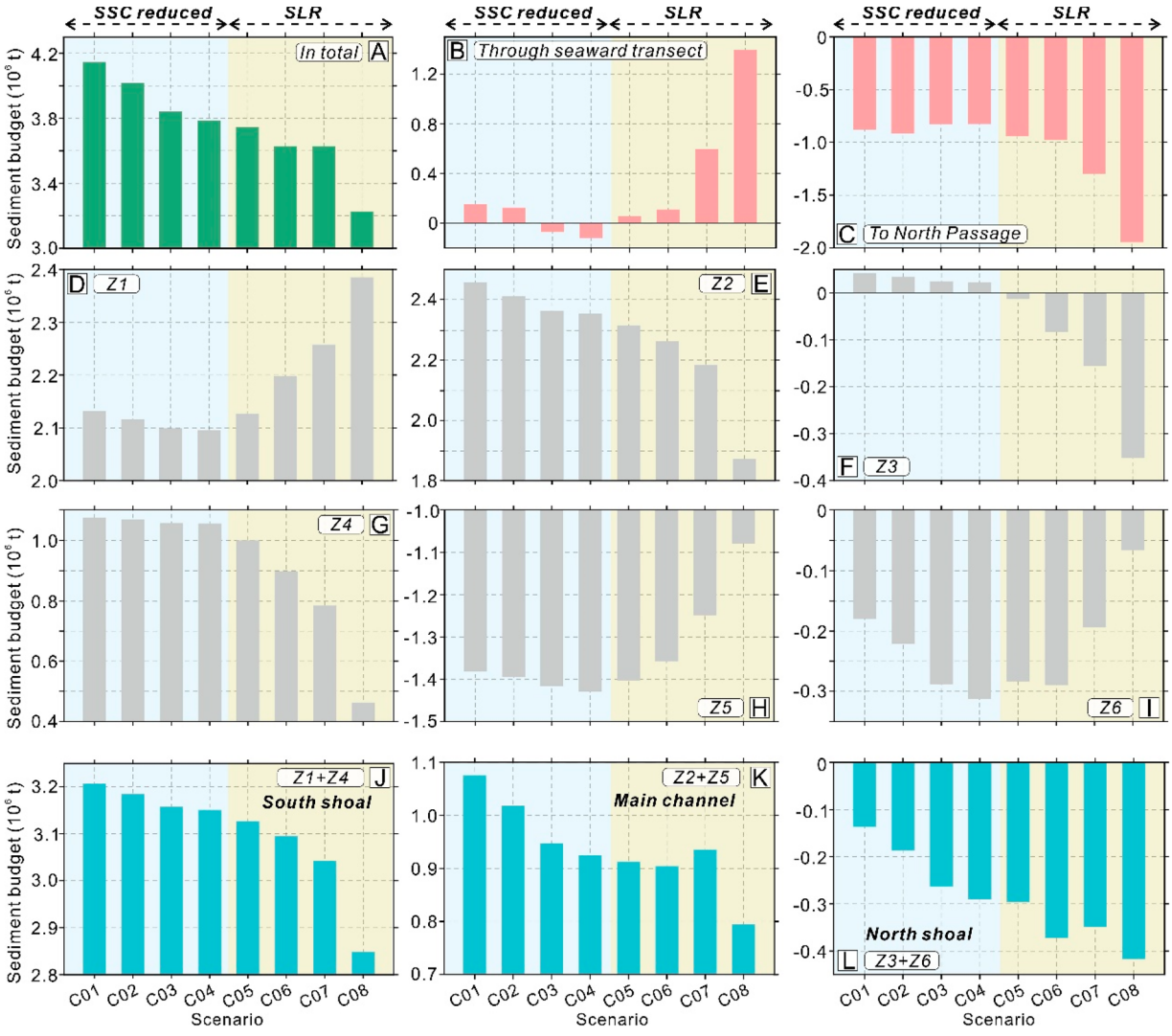

Figure 8. (A-I) Statistics of modeled net suspended sediment budgets in the entire area and different sub-zones in Scenarios C01–C08 (under gradually reduced SSC and SLR). (J-L) Net suspended sediment budgets in the south shoal, main channel and north shoal were also calculated.

and 4.06%, respectively, compared with Scenario C04 (no SLR) (Table 3). The spatial pattern of modeled flow velocity within the channel and shoals remained relatively stable (Figure S2). Results of Scenario C08 and Scenario C04 showed that the most increase in velocity (over 0.03 m/s) was located in the south Nanhui Shoal and most of the Jiuduansha Shoal (Figure 9A). The minor reductions (0–0.04 m/s) were mainly concentrated in the deepest upper South Passage channel and downstream of the mouth bar (Figure 9A). In addition, the modeled bed shear stress grew by 0.25%, 0.80%, 1.35% and 2.73%, respectively (Figure S3; Table 3). Here, the difference was that the extent of increased bed shear stresses receded within the Nanhui Shoal, Jiuduansha Shoal, and offshore areas, but the extent of reduced bed shear stress widened also bounded by the mouth bar (Figure 9B).

In addition, the modeled mean SSCs following SLR reduced by −0.95%, −3.07%, −4.27%, and −7.00% in the channel-shoal complex in Scenarios C05–C08, respectively (Figure S4; Table 3). The comparison between Scenario C08 and C04 suggested that the most obvious reduction occurred in the main deeper South Passage channel, its intensity gradually weakened towards the mouth bar and offshore areas (Figure 9C). Areas of reduction over $-0.06\ kg/m^3$ stretched downstream along the seaward edge of the Nanhui Shoal (Figure 9C). SSCs increased on the tail of the Jiuduansha Shoal, which were located in the sheltered areas adjacent to the south training wall of the Deep-water Navigation Channel Project in the North Passage (Figure 9C).

4.3.2. Variations in the suspended sediment budgets

After an SLR of 5 cm in Scenario C05, the modeled net aggradation in the study area declined by −1.11% to 3.744×10^6 t relative to Scenario C04, following similar trends from SSC input reductions (Figure 8A and

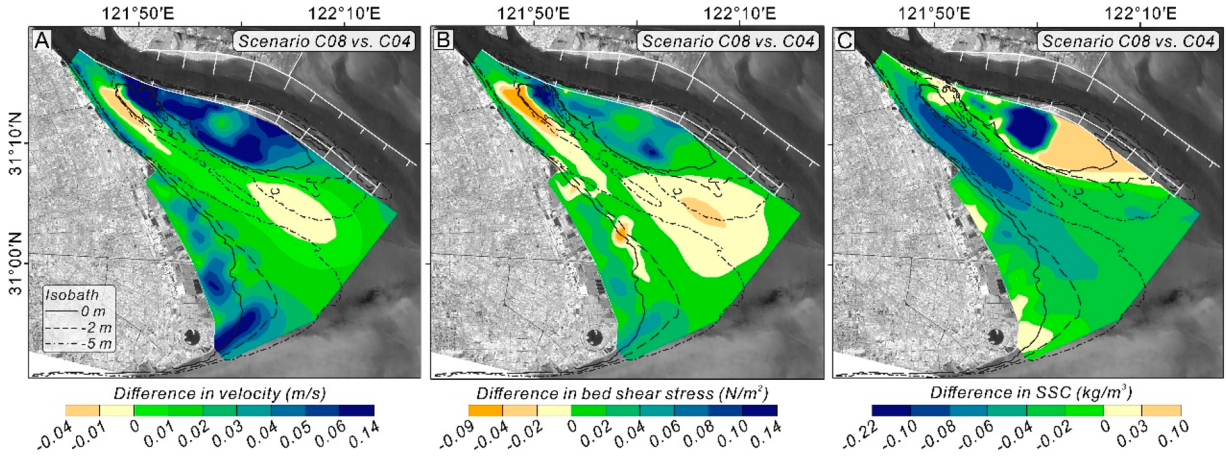

Figure 9. Differences in modeled mean depth-averaged velocity, bed shear stress and SSC between Scenario C08 (SLR of 50 cm) and Scenario C04 (no SLR).

Figure 10A). In particular, the total sediment fluxes along seaward transects shifted from the previous output to input from the sea, reaching 0.058×10^6 t; the flux exported to the North Passage increased by 14.30% to 0.943×10^6 t (Figure 8B-C; Table 4). The net deposition in sub-zones Z1 increased by 1.47%, which was the opposite of that caused by reduced SSC (Figure 8D and Figure 10A). However, the net deposition of the previously trapped sub-zones Z2 and Z4 continued to decrease by −1.65% and −1.59%, respectively, mainly corresponding to the locations of increased velocity and bed shear stress (Figure 8E and G). The suspended sediment budget in sub-zone Z3 turned from slight deposition to net export, and net outputs in sub-zones Z5 and Z6 lowered by −1.86% and −9.39%, respectively (Figure 8E–I).

With the SLR of 15 and 25 cm in Scenarios C06 and C07, the net trapped suspended sediment was further decreased by −4.18% and −4.16% to 3.628×10^6 t and 3.629×10^6 t (Figure 8A). Although the total difference between two scenarios within the overall complex was small, variations in different sub-zones were distinct. Herein, the net landward transport along seaward transects was 0.91 and 9.31 times greater than that in Scenario C05; the net transport amounts to the North Passage increased by 19.67% and 57.58%, respectively (Figure 8B-C and Figure 10B-C). Suspended sediment trapping in Sub-zone Z1 lowered by 4.85% and 7.72% (Figure 8D). SLR resulted in an exacerbated decrease in net deposition in sub-zones Z2 and Z4; increased the output in sub-zone Z3 by 4.68 and 7.87 times compared to Scenario C05 (Figure 8E-G). The net exports from sub-zones Z5 and Z6 also weakened (Figure 8H-I). In Scenario C08, the net trapped suspended sediment was further reduced by 14.79% to 3.226×10^6 t (Figure 8A and Figure 10D). Correspondingly, the landward flux through seaward transects amounted to 1.393×10^6 t, which is 23.07 times that of scenario C05 (Figure 8B and Figure 10D). Hence, the downstream sub-zones Z5 and Z6 experienced a significant reduction in net output of −24.52% and 78.82%, respectively (Figure 8H-I). While the trapping efficiencies in sub-zones Z2 and Z4 diminished by −20.42% and 56.07% (Figure 8D-E and G).

Overall, the SLR simulations indicate a decrease in the net suspended sediment trapping in the entire channel-shoal complex, which is similar to the tendency with reduced riverine SSC inputs (Figure 8A). Differences remain. (1) A lower SSC resulted in a gradual reduction in suspended sediment deposition in sub-zones Z1–Z4, whereas SLR enhances deposition in sub-zones Z1 (Figure 8D-G). (2) Sediment gains in sub-zone Z2 and sub-zone Z4 were further weakened with SLR; especially in sub-zone Z3 in the upper Jiuduansha Shoal, which shifted from a slightly weak net input to an increased output (Figure 8E–G and Figure 10). (3) SLR lowers the net export of suspended sediment to downstream sub-zones Z5–Z6 (Figure 8H-I and Figure 10).

4.4. Superimposed effects with lower SSC

The combined effects of SSC reduction and SLR result in a further lowering of the SSC. When the SSC input at Datong station was reduced to 0.06 kg/m^3, the mean of modeled SSC in Scenarios C09 and C10 was lower by −0.30% and 0.25% relative to Scenarios C06 and C08 (Table 3). The greatest reduction in SSC was concentrated at the upstream entrance of the South Passage, the magnitude gradually weakened toward the mouth bar and strengthened again in the offshore areas (Figure 5). Therefore, the net suspended sediment trapping amount was 3.579×10^6 t and 3.206×10^6 t, respectively, which was −1.36% and −0.63% less relative to scenarios C06

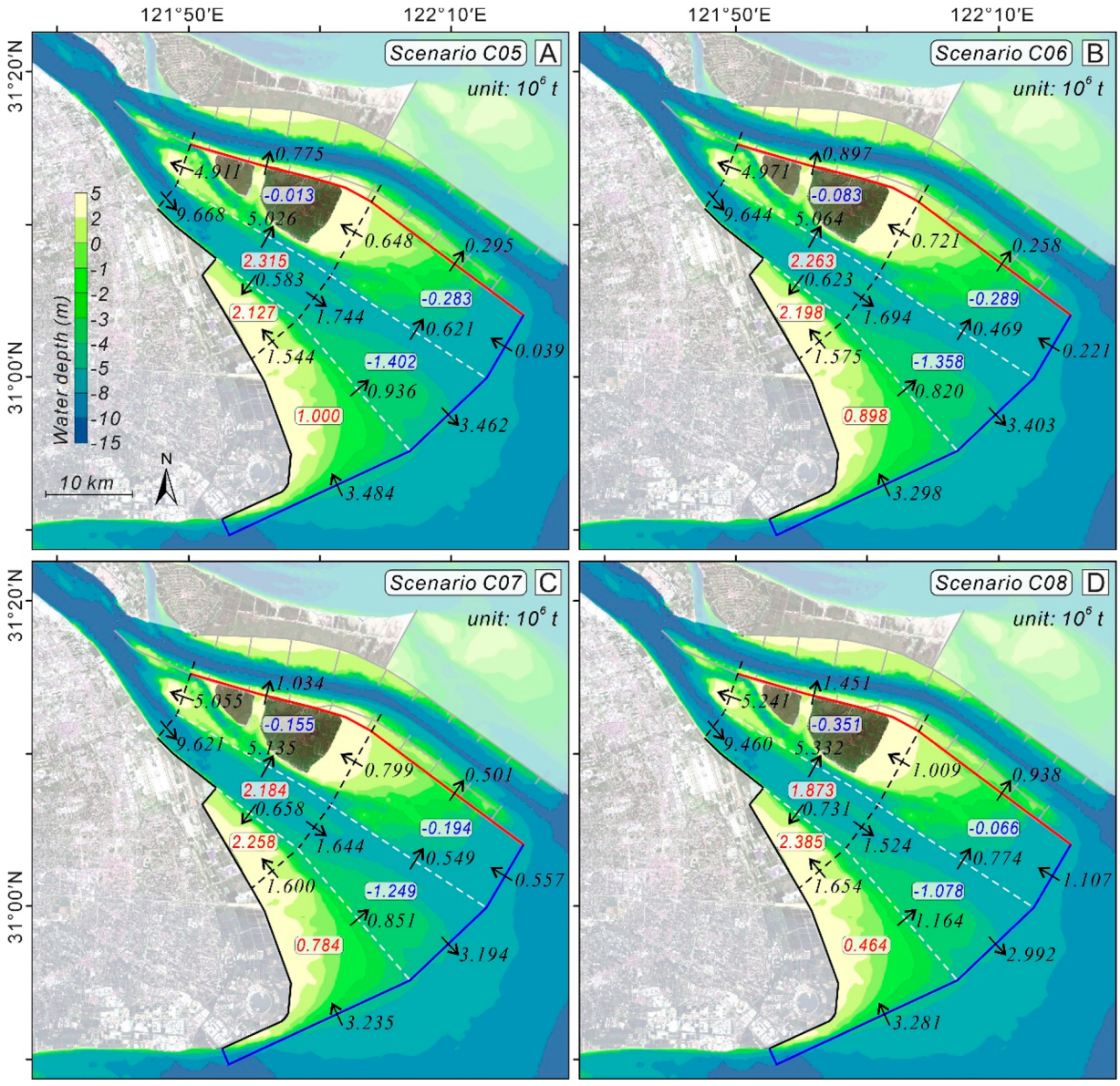

Figure 10. Modeled suspended sediment fluxes and net budgets within different sub-zones in Scenarios C05–C08 (SLRs of 5, 15, 25 and 50 cm, respectively).

and C08 (Figure 11). The total landward sediment flux along the seaward transect was reduced by −2.83% and −3.30% (Table 4). Only the output from sub-zones Z3 and Z6, close to the south training wall of the Deep-water Navigation Channel Project in the North Passage, was reduced; the net input or net output in other sub-zones was weakened or enhanced (Figure 11) (Table 5).

Table 5. Variation in net suspended sediment budgets in the entire study area and three sub-regions under the impact of SLR (C06 and C08) and superimposed further lower SSC (C09 and C10).

Scenario	Total (10^6 t)	South shoal (10^6 t)	Main channel (10^6 t)	North shoal (10^6 t)
C04	3.786	3.151	0.925	−0.290
C06	3.628	3.096	0.905	−0.372
C08	3.226	2.849	0.795	−0.417
C09	3.579	3.088	0.883	−0.392
C10	3.206	2.843	0.787	−0.424

5. Discussion

5.1. Impact of reduced riverine sediment supply

Since the Holocene, large amounts of river-derived sediments have accumulated in fluvial-tidal environments (Bianchi & Allison, 2009; Goodbred & Kuehl, 1999). For instance, about 80% of riverine sediment was captured in the Mekong Delta over the past three millennia, which allowed it to grow and become a place of great socio-ecological importance (Szczuciński et al., 2013; Xue et al., 2010). Maintaining stability in these mega-deltaic channel-shoal complexes is therefore

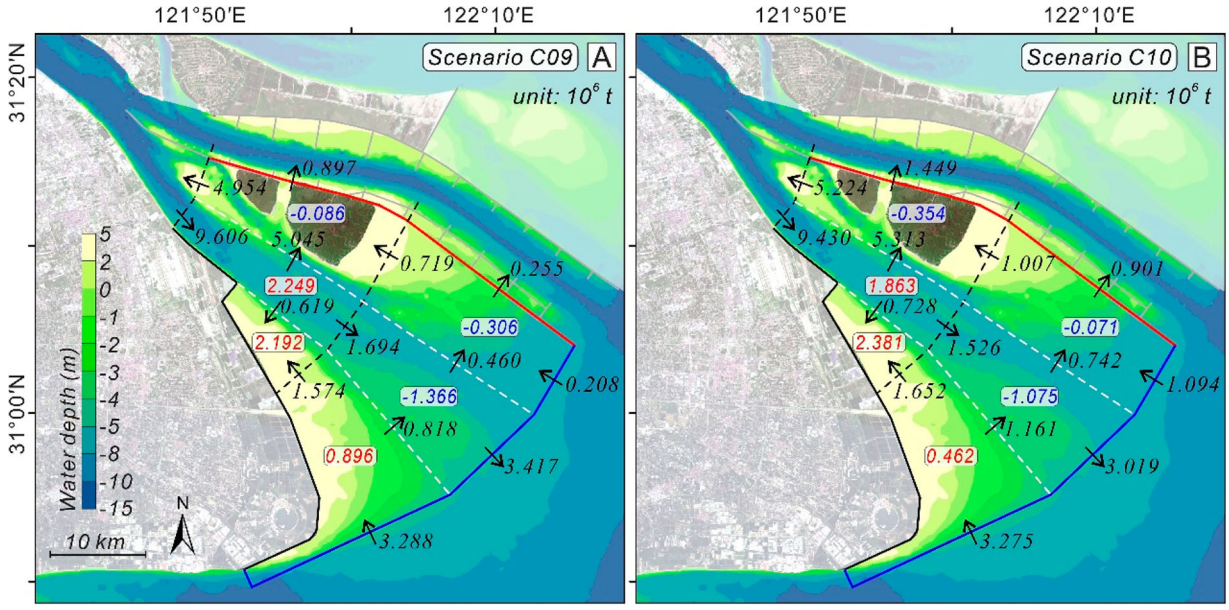

Figure 11. Modeled suspended sediment fluxes and corresponding net budgets within different sub-zones in Scenarios C09–C10 (SLRs of 15 and 50 cm with the riverine SSC is further reduced to 0.06 kg/m^3).

paramount (Allison, 1998; Anthony et al., 2014; Syvitski et al., 2009). Recent enhanced variability of the terrestrial sediment supply and associated declining SSC triggered by global climate change and human activities strongly affect sediment budgets and deltaic geomorphology (Blum & Roberts, 2009; Dai et al., 2014; Nienhuis et al., 2020; Raff et al., 2023).

For example, in the mega Ganges-Brahmaputra Delta, modern sediment dispersal patterns were similar to those in the past; although continuous deposition occurred in disparate depocenters, and parts of the delta are eroding (Akter et al., 2021; Goodbred & Kuehl, 1999). The Red River Delta was rapidly growing owing to the abundance of climate-driven sediment. Nhuan and Van Ngoi (2012) indicated that the upstream construction of hydraulic projects would reduce sediment availability and exacerbate erosion-stressed geomorphic stability. In the mega-Mekong, over 50% of the coastline experienced erosion and land loss between 2003 and 2012; the tidal intrusion will advance landward over 50 km in the next two decades due to channel erosion after reduced river SSC, which will most likely be worsened by sediment starvation and SLR (Anthony et al., 2015; Vasilopoulos et al., 2021). In deltas overall, the reduced upstream sediment supply, sand mining, and land reclamation will intensify the shift in sediment budget from deposition to export, alter hydrodynamic conditions and runoff-tidal equilibrium locations between the deep channel and tidal shoals (Chen et al., 2022; Cox et al., 2021).

In the Changjiang Delta, tides are the dominant driver controlling the development of the channel-shoal morphology but accelerated progradation over the past 2000 years of BP can be attributed to the increased riverine sediment supply (Chen et al., 1979; Gao et al., 2019; Hori et al., 2001). However, since the Three Gorges Dam was constructed in 2003, the sediment retention rate in the entire Changjiang Delta has been reduced to the 30% (0.49×10^8 t/yr) of the average during the previous two millennia (Hori et al., 2002; Wang et al., 2018b). The mean SSC at Datong dropped from 0.53 kg/m^3 between 1965 and 1988 to 0.122 kg/m^3 between 2014 and 2022 (Text S1). Consequently, the sediment budgets and geomorphic change within the channel-shoal complex shifted to achieve a new equilibrium (Dai et al., 2014; Liu et al., 2007 & 2018a). Studies have indicated that the distributary channels and tidal shoals are already experiencing erosion due to lowered water discharge and that the extent of sediment sinks turning into sources is expanding (Gao et al., 2019; Xie et al., 2017). The Changjiang Delta was eroding at −5.59 cm/yr between 2007 and 2019, in particular, channels deeper than −10 m eroded while tidal shoals shallower than −5 m experienced accretion (Guo et al., 2021).

The results of this study confirmed that the strong incision in the upper South Passage and enhanced erosion of the mouth bar and offshore areas over the past 40 years (Figures 3 and 4). Both the measured net deposition rate and the modeled suspended sediment trapping efficiency gradually decreased, which can be attributed largely to the continued reduction in SSC from the Changjiang River (Dai et al., 2015; Wei et al., 2017; Yang et al., 2005). Geomorphic evolution of the South

Passage shifted from an erosion state before 2003 to partially infilling and formed a two-channel configuration, this tendency was enhanced by the full operation of the Three Gorges Dam (Dai et al., 2015; Luo et al., 2023; Mei et al., 2021). Moreover, with the continued erosion in the Changjiang Delta and net export of fine-grained sediments, the sediment coarsening in the delta-shelf transition zone also provided sedimentologic evidence for delta degradation resulting from its sediment deficits (Zhan et al., 2020; Zou & Gao, 2019).

5.2. Effect of SLR on deltaic suspended sediment budgets

Global mean SLR was 2.6 mm/yr during the past two decades. With likely future accelerating SLR, the resilience of coastal zone populations and ecosystems is severely tested (Cazenave & Cozannet, 2014; Nicholls et al., 2021). Sea-level change can make or break mega fluvial-tidal deltas, and with future SLR the channel-shoal geomorphic complex of the Changjiang Delta is more vulnerable to transgression (Nienhuis et al., 2023; Porebski & Steel, 2006). SLR can also change waves and tidal forcings and further increase delta inundation and shoreline migration (van De Lageweg & Slangen, 2017). For instance, by 2100, SLR might trigger a 67% increase in tidal amplitude along the northern Gulf of Mexico and accelerate the propagation rate of tidal currents in the bays and estuaries (Passeri et al., 2016). In the Mekong delta, the combined effects of channel incisions caused by reduced river sediment supply and SLR led to an increase in M_2 tidal amplitude of 1.1–2.0 and 2.0 cm/yr in the offshore and inland areas, respectively, which enhanced saltwater intrusion into the delta along distributaries (Erban et al., 2014; Eslami et al., 2019).

In general, SLR-induced increases in the relative tidal energy will result in altered sediment transports and budgets in most mega-deltas (Allison, 1998; Khan et al., 2020). These changes then work their way through delta morphologic changes, and, in many cases, result in stronger tides that may locally amplify the threat of SLR (Finotello et al., 2019; Ibàñez et al., 1997). For example, the Eastern Scheldt Estuary will shift to ebb dominance when SLR increases up to 2.0 m, which will accelerate tidal currents and promote a net export of sand (Jiang et al., 2020). In the mesotidal Deben Estuary, SLR will intensify hydrodynamic-geomorphic changes around the ebb delta (Yin et al., 2019). Overall, SLR-enhanced tidal currents could be the critical driver of erosion in a deltaic channel-shoal system; with a shift of sediment deposition upstream toward the fluvial sediment source because of the greater flood tide dominance (Elmilady et al., 2022; van Maanen et al., 2013).

In the mega-Changjiang Delta, changes in the relative strength of river discharge and tides can lead to variations in the transport patterns, with the offshore depocenter moving northward due to stronger tidal forcings (Dai et al., 2014; Yun, 2004; Zhu et al., 2020). In addition, SLR can increase tidal levels in the Changjiang Delta and accelerate the propagation of tidal currents toward the upstream deltaic channels, which may enhance tidal shoal erosion (Kuang et al., 2014). Numerical modeling suggested that SLR lowers the net sediment export in the mouth bar of the Changjiang Delta, while an increased M_2 tidal component led to increased output (Chu et al., 2020). Tidal skewness (γ) (Eq. 12) can quantify the changes in tidal forcing due to SLR, with the positive and negative values representing flood-dominance and ebb-dominance:

$$\gamma = \frac{\frac{1}{T-1}\sum_{t=1}^{T}(x_t - \bar{x})^3}{\left[\frac{1}{T-1}\sum_{t=1}^{T}(x_t - \bar{x})^2\right]^{3/2}} \tag{12}$$

where x_t is the derivative of the water level with respect to time t, and $\bar{x}$ is the mean water level. Model scenarios C04–C08 indicated mostly ebb-dominant conditions along the thalweg of the South Passage, and a decrease in ebb-dominance toward the sea. SLR reduces the ebb-dominance and leads to flood-dominant conditions offshore of the South Passage (Figure 12). Therefore, SLR generates stronger flood tides and suppresses the prevailing ebb-dominance (Kuang et al., 2014; Shen & Li, 2011; Wang et al., 2023). The effect of SLR on the tidal skewness is further illustrated by modeled total suspended sediment flux through three seaward transects herein. The flux shifted from negative to positive due to SLR in this study, suggesting that more suspended sediment is being imported into the upper deltaic channel from the offshore areas (Figure 8B).

Results in Table 3 and Figure S5 show that in scenarios C09–10 although the SSC from the Changjiang River has been further reduced to 0.060 kg/m^3, the overall means of SSC in the channel-shoal complex only slightly lower than that of scenarios C06 and C08 with the same SLR. This is partly related to its location in the Maximum Turbidity Zone in the Changjiang Delta, where the SSC is higher due to the mixing effect and stratification of fresh and saltwater (Chen et al., 1988; Li et al., 1994; Shen et al., 1992 and 2010). Some studies have suggested that SLR can favor the formation of Maximum Turbidity Zone in mega-deltas and weaken the ebb-tide dominance, thereby reducing net sediment transport to the sea (Allison et al., 2017; Chu, 2019; van Maanen et al., 2013). Moreover, it needs to be stressed that with global/regional climate change and enhanced human disturbances (damming, water withdrawals, etc.)

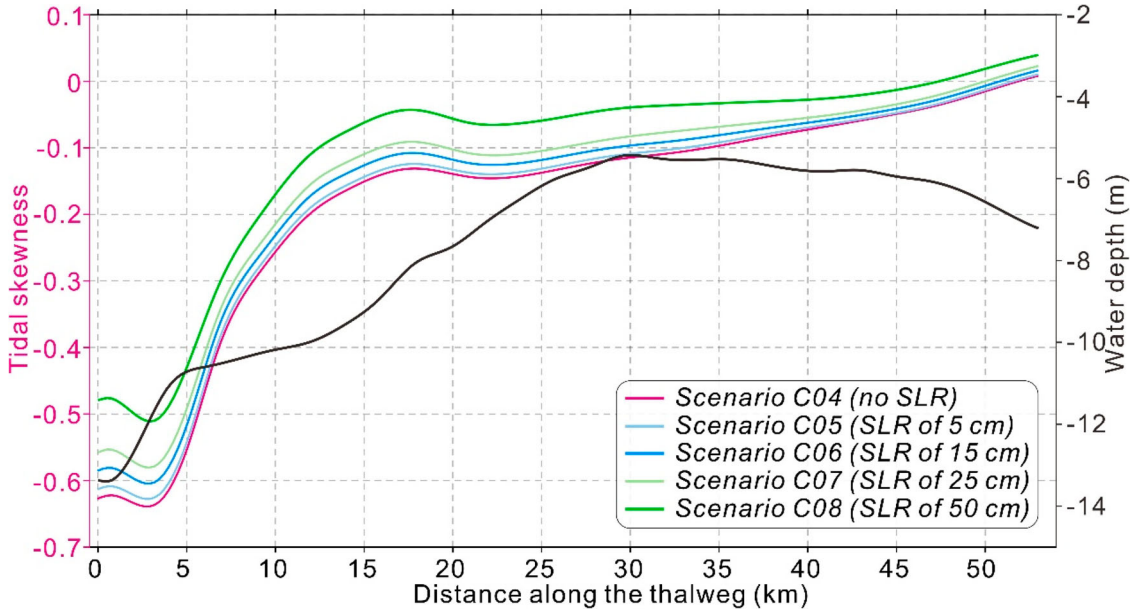

Figure 12. Calculated tidal skewness along the thalweg in Scenarios C04–C08, the longitudinal variation of bathymetric depth was also shown.

in the basin, water discharge entering into the Changjiang Delta is most likely to decrease gradually along with rising sea levels, which possibly aggravating the lack of terrestrial sediment supply (Dai, 2021; Luan et al., 2017). Thus, deltaic sediment transport and geomorphic changes affected by coupled changing river and marine drivers are attracting global attention (Hoitink et al., 2017; Nienhuis et al., 2018; Raff et al., 2023).

Studies have indicated that fine-grained sediments accumulated in the delta front and subaqueous areas can be re-transported landward by SLR-enhanced tides, which will be an important and new sediment source to feed the growths of delta shoals (Akter et al., 2021; Fagherazzi et al., 2020; Kuehl et al., 1986; Szczuciński et al., 2013). Thus, sediment redistribution and geomorphic adjustments in the delta channel-shoal system have attracted more widespread attention (Leonardi et al., 2021; Nienhuis et al., 2018; Passeri et al., 2015; van Maanen et al., 2013). For example, model results from California suggest that SLR and reduced sediment supply may move the primary location of sediment deposition from the San Francisco Bay to the San Pablo Bay further upstream (Elmilady et al., 2019; van der Wegen et al., 2017). This is similar to the findings in this study, where SLR led to an increase in overall sediment export, but net seaward exports from the downstream sub-zones Z5–Z6 declined (Figure 8). One reason for this could be the duration of the flood tide. An SLR of 0.5 m resulted in an increase in this duration of 1.18%, 1.23%, and 3.64% at the three sites (H1, H2, and H3) in the South Passage (Figure 13; Table 6). Mean bed shear stress increased by 0.30% and 0.39% during the flood tide at the H2 and H3 sites, respectively (Figure 13; Table 6). Mean bed shear stress at the site of the Jiuduansha Shoal and Nanhui Shoal (H2-N, H2-S) also increased with SLR; and the former resulted in a reduction of suspended sediment deposition (Figures 8 and 14; Table 6).

Table 6. Variations (magnitude, angle and duration) in modeled bed shear stress during the flood and ebb tides under the influence of SLR at five sites.

		Bed shear stress (N/m^2)		Angle (°)		Duration (%)	
Site	Scenario	Flood	Ebb	Flood	Ebb	Flood	Ebb
H1	*C04*	0.80	0.84	329.68	149.13	46.81%	53.19%
	C06	0.79	0.87	330.21	149.03	47.09%	52.91%
	C08	0.78	0.93	329.67	148.44	47.37%	52.63%
	C08 vs. C04	−1.41%	9.62%	0.00%	−0.47%	1.18%	−1.04%
H2-N	*C04*	0.16	0.16	267.46	120.49	54.85%	45.15%
	C06	0.18	0.15	279.58	119.67	53.74%	46.26%
	C08	0.21	0.15	292.62	116.86	52.35%	47.65%
	C08 vs. C04	24.96%	−3.90%	9.41%	−3.01%	−4.55%	5.52%
H2	*C04*	0.40	0.51	313.62	122.26	44.88%	55.12%
	C06	0.40	0.50	313.24	121.54	45.15%	54.85%
	C08	0.40	0.49	313.55	119.77	45.43%	54.57%
	C08 vs. C04	0.30%	−3.97%	−0.02%	−2.04%	1.23%	−1.01%
H2-S	*C04*	0.24	0.18	257.29	67.76	38.23%	61.77%
	C06	0.25	0.18	257.70	70.58	37.67%	62.33%
	C08	0.24	0.17	253.87	71.45	39.06%	60.94%
	C08 vs. C04	0.41%	−3.95%	−1.33%	5.44%	2.17%	−1.35%
H3	*C04*	0.46	0.46	286.51	107.33	45.71%	54.29%
	C06	0.46	0.45	287.23	107.37	45.98%	54.02%
	C08	0.46	0.45	286.90	106.29	47.37%	52.63%
	C08 vs. C04	0.39%	−0.61%	0.13%	−0.97%	3.64%	−3.06%

5.3. Implications for future deltaic morphodynamics

In the last centuries, high-intensity human activities emerged as the critical drivers impacting hydrodynamics

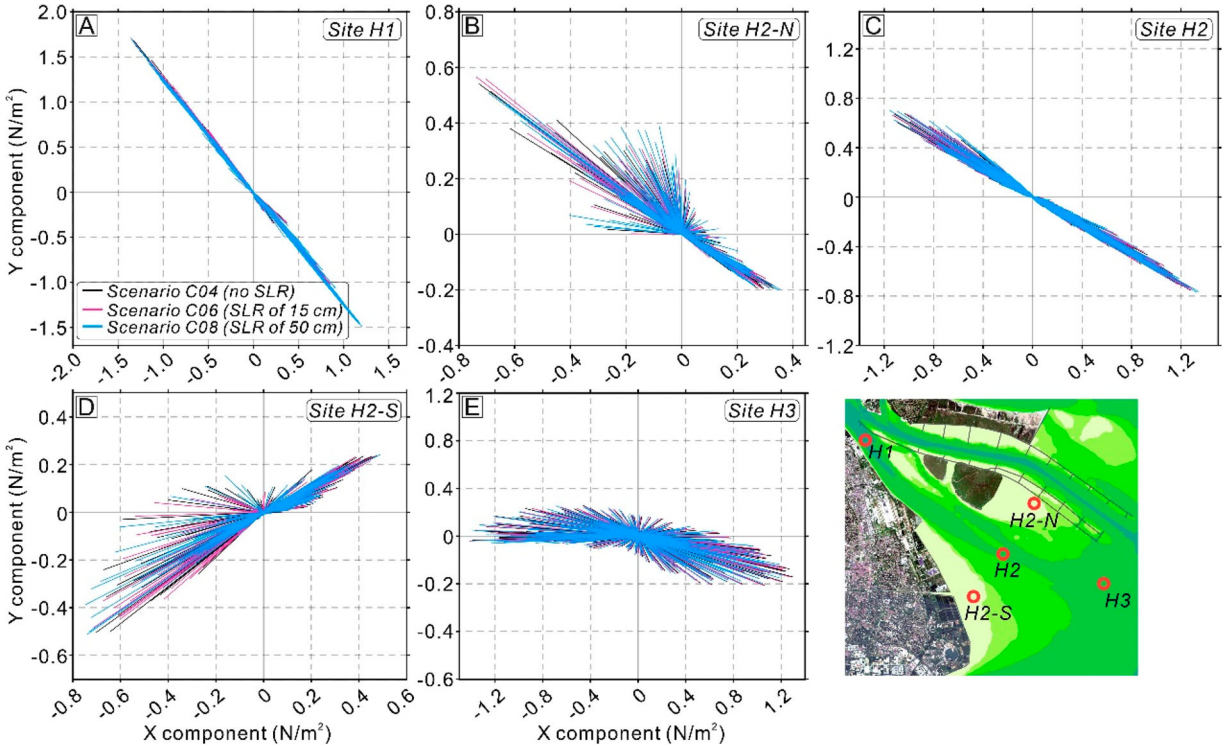

Figure 13. The vectors and changes of modeled bed shear stress during the spring-neap tidal periods at different five fixed sites in Scenarios C04, C06 and C08.

and sediment budgets in mega-deltas (Anthony et al., 2014; Ericson et al., 2006). Channelization works prevented avulsions in the Rhône Delta and likely exacerbated erosion of the prodeltaic lobes (Sabatier et al., 2009). Vellinga et al. (2014) found a human-driven reduction of extreme water levels in the Rhine-Meuse Delta since 1940, despite the SLR. In addition, land reclamation might lead to marine sediment import, despite sediment deficits in tide-influenced subaqueous deltas (Angamuthu et al., 2018). For instance, in the Guayas River Estuary, Gulf of Guayaquil, artificial reclamations increased the flood tidal currents, thus leading to greater input of seaward sediment (Barrera Crespo et al., 2019). These examples are visible on a global scale. While not all deltas have lost land over the past three decades, deltas that shifted to a more pronounced tidal dominance were gaining land (Nienhuis et al., 2020).

In the Changjiang Delta, the tidal flats on both sides of the South Passage channel, i.e. the Nanhui Shoal and Jiuduansha Shoal, both showed relatively natural states until 1990 (Figure 14A–C). However, the construction of the Deep-water Navigation Channel Project in the North Passage since 1998 has dramatically altered flow and sediment transport in the Jiuduansha Shoal, with affected the bathymetry and the marshes (Li et al., 2016; Wei et al., 2016). The added effect of the diversion works of the Deep-water Navigation Channel Project also resulted in a higher flow entering the South Passage channel, and the south training walls obstructed the propagation of flood tides toward the North Passage (Jiang et al., 2012). Together with the increased runoff and lower SSC feeding the delta, this caused erosion in the upper South Passage, which expanded downstream toward the mouth bar and offshore areas (Figures 3 and 4). In addition, the progradation rate in the Nanhui Shoal accelerated because of substantial intertidal-subtidal enclosures, meanwhile, seaward erosion induced steeper topographic gradients (Wang et al., 2018; Wei et al., 2017; Zhang et al., 2018b; Wang et al., 2022a).

Specifically, the upper intertidal Nanhui Shoal was reclaimed (totaling 134 km^2) between 1994 and 2002 and increased sedimentation; the first stage of the Deep-water Navigation Channel Project also allowed some sediment to be trapped in groins and the south training wall (Figure 14D–I). The second and third stage engineering of the navigation channel and the latest siltation-promoting projects (150 km^2) in the Nanhui Shoal have been carried out, thus resulting in more sediment retention, and further erosions in subaqueous areas (Figures 4 and 14D–I). Hence, the bathymetry in the deltaic channel and tidal shoals in the southern Changjiang Delta are severely disturbed at present. Mei et al. (2023) suggested that tidal flat accretion in the Nanhui Shoal may decelerate when available sediment falls below a threshold of

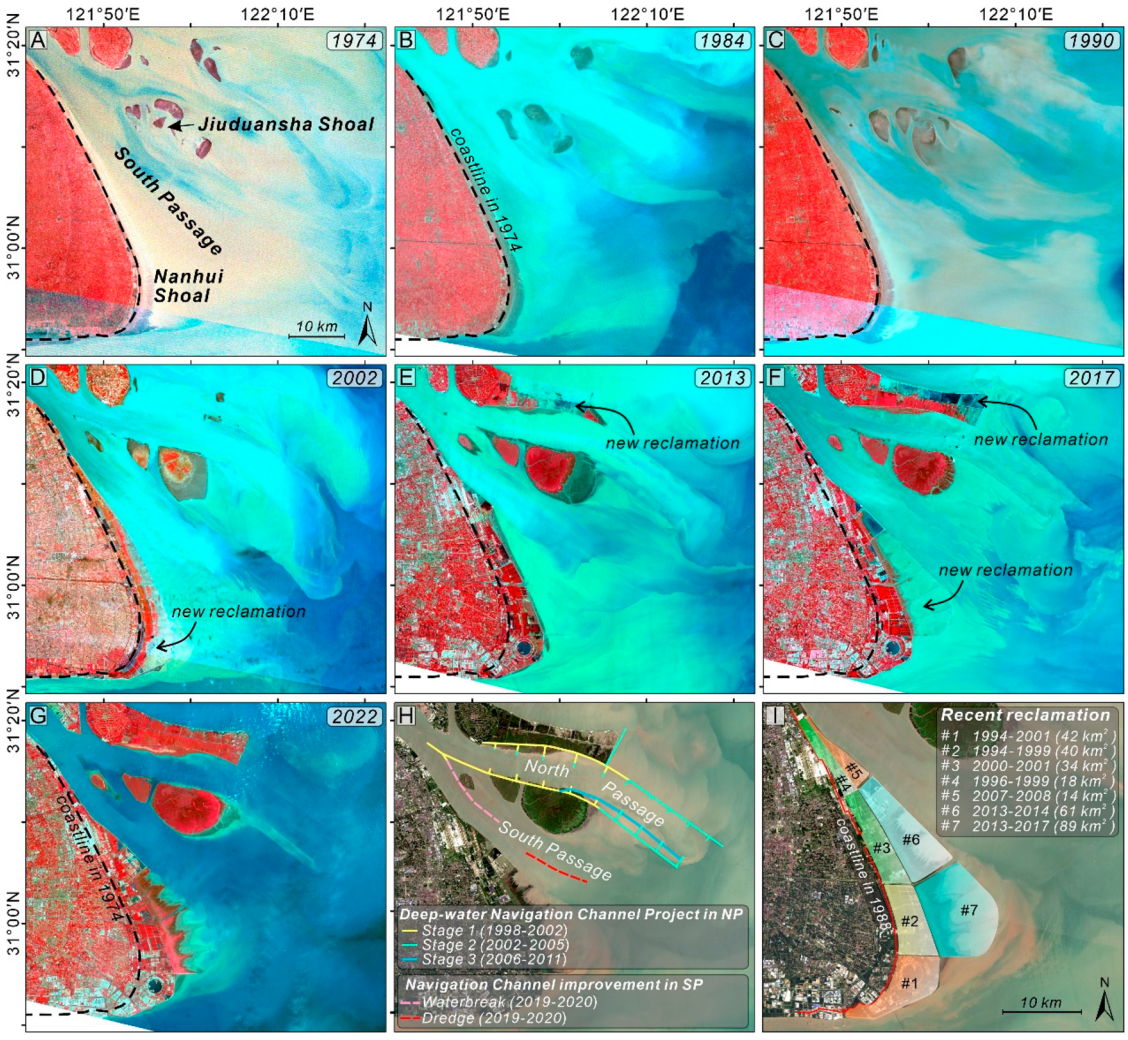

Figure 14. (A-G) Changes in the coastline and anthropogenic disturbances in the study area between 1974 and 2022 were illustrated by Landsat satellite imageries. (H) The Deep-water Navigation Channel Project with multiple jetties-groins was constructed in the North Passage between 1998 and 2011, and the latest breakwater and dredging was carried out in the South Passage between 2019 and 2020. (I) Recent reclamation areas along the Nanhui Shoal over the past 30 years reached 300 km^2.

0.01×10^8 t/y, with enhanced erosion in the South Passage channel and south Jiuduansha Shoal (Dai, 2021; Gao et al., 2019; Guo et al., 2021).

In the future, it is undeniable that the accretion and progradation of tidal shoals in natural or semi-natural states will be challenged (Ibàñez et al., 1997). Riverine sediment deficits, rapid SLR, and further anthropogenic activity may lead to global deltaic land loss of 5% and 50% by 2100 and 2300 under the RCP8.5 Scenarios, respectively (Nienhuis et al., 2023; Nienhuis & van de Wal, 2021). Moreover, new damming and coastal infrastructure will further restrict sediment retention and land elevation gain in 46 mega-deltas (Tessler et al., 2018). In particular, hydrodynamic, geomorphologic, and ecological responses induced by multiple threats are interrelated in fluvial-tidal deltas; synergetic approaches are needed to study sedimentary and morphodynamic changes (Fagherazzi et al., 2020; Passeri et al., 2015; Saintilan et al., 2022). Furthermore, there is also an urgent need to develop effective nature-based solutions to increase sediment accumulation and to strengthen the resilience of channel-shoal geomorphic complexes to cope with SLR in mega fluvial-tidal deltas (Raff et al., 2023; Schmitt et al., 2021; Tang, 2008).

6. Conclusions

Geomorphic changes in the South Passage, Nanhui Shoal, and Jiuduansha Shoal of the Changjiang Delta between 1979 and 2020 were examined here using bathymetric data. A process-based Delft3D numerical model was used to analyze the variations in suspended sediment budgets triggered by sediment reduction and SLR in this channel-shoal environment. The main conclusions are:

(1) After Three Gorges Dam-induced riverine SSC reduced by 75% in several stages, the net deposition rate within the entire complex decreased from 4.20 cm/yr in 1979–1990 and 3.21 cm/yr in 1990–2003, to 2.21 cm/yr in 2003–2013 and 0.40 cm/yr in 2013–2020.
(2) Channel erosion of over 2.0 m occurred along the upper South Passage during the past four decades, which extended longitudinally toward the mouth bar and offshore areas. Sedimentation of over 1.0 m accumulated in the bordering Nanhui Shoal and Jiuduansha Shoal, both of which have been influenced by engineering.
(3) Modeling results indicated that when the SSC from the Changjiang River was reduced from 0.53, to 0.35 kg/m^3, to 0.16 kg/m^3, and finally 0.12 kg/m^3, the net suspended sediment deposition herein was lowered by 3.13%, 7.35% and 8.67%, respectively. Sediment export increased from the northern shoals.
(4) Suspended sediment trapping efficiency within this complex was projected to continue to diminish by 1.11%, 4.18%, 4.16%, and 14.79% relative to present with an SLR of 5, 15, 25, and 50 cm, respectively.

As a typical fluvial-tidal delta, the mega-Changjiang Delta is affected by the superimposed effects of lower riverine SSC input and SLR, which will cause greater reductions in sediment budgets. The findings may provide insights into the broader morphodynamics and sediment budgets of global deltaic channel-shoal complexes that have to cope with sediment deficits and SLR.

Acknowledgments

This study was financially supported by the Joint Key Funds of National Natural Science Foundation of China under grant number U2040202; and the Shanghai International Science and Technology Cooperation Fund Project under grant number 23230713800. More details can be obtained from the corresponding author (zjdai@sklec.ecnu.edu.cn) upon reasonable request.

Disclosure statement

No potential conflict of interest was reported by the author(s).

Funding

This work was supported by Joint Key Funds of National Natural Science Foundation of China: [grant number U2040202]; Shanghai International Science and Technology Cooperation Fund Project: [grant number 23230713800].

References

Akter, J., Roelvink, D., & van der Wegen, M. (2021). Process-based modeling deriving a long-term sediment budget for the Ganges-Brahmaputra-meghna delta, Bangladesh. *Estuarine, Coastal and Shelf Science*, *260*, 107509. https://doi.org/10.1016/j.ecss.2021.107509

Allison, M. A. (1998). Historical changes in the Ganges-Brahmaputra delta front. *Journal of Coastal Research*, 1269–1275.

Allison, M. A., Nittrouer, C. A., Ogston, A. S., Mullarney, J. C., & Nguyen, T. T. (2017). Sedimentation and survival of the Mekong Delta: A case study of decreased sediment supply and accelerating rates of relative sea level rise. *Oceanography*, *30*(3), 98–109. https://doi.org/10.5670/oceanog.2017.318

Angamuthu, B., Darby, S. E., & Nicholls, R. J. (2018). Impacts of natural and human drivers on the multi-decadal morphological evolution of tidally-influenced deltas. *Proceedings of the Royal Society A*, *474*(2219), 20180396. https://doi.org/10.1098/rspa.2018.0396

Anthony, E. J., Brunier, G., Besset, M., Goichot, M., Dussouillez, P., & Nguyen, V. L. (2015). Linking rapid erosion of the Mekong river delta to human activities. *Scientific Reports*, *5*(1), 14745. https://doi.org/10.1038/srep14745

Anthony, E. J., Marriner, N., & Morhange, C. (2014). Human influence and the changing geomorphology of Mediterranean deltas and coasts over the last 6000 years: From progradation to destruction phase? *Earth-Science Reviews*, *139*, 336–361. https://doi.org/10.1016/j.earscirev.2014.10.003

Barrera Crespo, P. D., Mosselman, E., Giardino, A., Becker, A., Ottevanger, W., Nabi, M., & Arias-Hidalgo, M. (2019). Sediment budget analysis of the Guayas River using a process-based model. *Hydrology and Earth System Sciences*, *23*(6), 2763–2778. https://doi.org/10.5194/hess-23-2763-2019

Becker, M., Papa, F., Karpytchev, M., Delebecque, C., Krien, Y., Khan, J. U., Ballu, V., Durand, F., Cozannet, G. L., Saiful Islam, A. K. M., Calmant, S., & Shum, C. K. (2020). Water level changes, subsidence, and sea level rise in the Ganges-Brahmaputra-Meghna delta. *Proceedings of the National Academy of Sciences*, *117*(4), 1867–1876. https://doi.org/10.1073/pnas.1912921117

Bianchi, T. S., & Allison, M. A. (2009). Large-river delta-front estuaries as natural "recorders" of global environmental change. *Proceedings of the National Academy of Sciences*, *106*(20), 8085–8092. https://doi.org/10.1073/pnas.0812878106

Blum, M. D., & Roberts, H. H. (2009). Drowning of the Mississippi delta due to insufficient sediment supply and global sea-level rise. *Nature Geoscience*, *2*(7), 488–491. https://doi.org/10.1038/ngeo553

Caldwell, R. L., & Edmonds, D. A. (2014). The effects of sediment properties on deltaic processes and morphologies: A numerical modeling study. *Journal of Geophysical Research: Earth Surface*, *119*(5), 961–982. https://doi.org/10.1002/2013JF002965

Cazenave, A., & Cozannet, G. L. (2014). Sea level rise and its coastal impacts. *Earth's Future*, *2*(2), 15–34. https://doi.org/10.1002/2013EF000188

Changjiang Water Resources Commission. (2022). *Changjiang river sediment bulletin*. Changjiang Press.

Chen, J. Y., Li, D. J., Chen, B. L., Hu, F. X., Zhu, H. F., & Liu, C. Z. (1999). The processes of dynamic sedimentation in the Changjiang Estuary. *Journal of Sea Research*, *41*(1-2), 129–140. https://doi.org/10.1016/S1385-1101(98)00047-1

Chen, J. Y., Shen, H. T., & Yun, C. X. (1988). *Hydrodynamics and geomorphic evolution in the Yangtze (Changjiang) Estuary*. Shanghai Science and Technology Press. in Chinese.

Chen, J. Y., Yun, C. X., Xu, H. G., & Dong, Y. F. (1979). The developmental model of the Chang Jiang river estuary during last 2000 years. *Haiyang Xuebao*, *1979*(*1*), 103–111.

Chen, K. L., He, Z. X., Liu, J., Lin, Y. T., & Jia, L. W. (2022). Long-term morphological evolution and its mechanism of Lingdingyang estuary: Interferences from anthropogenic forcings. *Marine Geology*, *450*, 106856. https://doi.org/10.1016/j.margeo.2022.106856

Chu, A. (2019). *Analysis and modelling of morphodynamics of the Yangtze Estuary*. Doctoral dissertation. Delft University of Technology.

Chu, A., Tai, J. A., Chen, Y. P., & Wang, B. (2020). Sediment budget of the mouth Bar in the Yangtze estuary response to the change of marine input conditions: A process-based model approach. *Journal of Coastal Research*, *105*, 36–41.

Chu, A., Wang, Z. B., & de Vriend, H. J. (2015). Analysis on residual coarse sediment transport in estuaries. *Estuarine. Coastal and Shelf Science*, *163*, 194–205. https://doi.org/10.1016/j.ecss.2015.06.003

Cox, J. R., Huismans, Y., Knaake, S. M., Leuven, J. R. F. W., Vellinga, N. E., van der Vegt, M., Hoitink, A. J. F., & Kleinhans, M. G. (2021). Anthropogenic effects on the contemporary sediment budget of the lower Rhine-Meuse Delta channel network. *Earth's Future*, *9*, e2020EF001869.

Dai, Z. J. (2021). *Changjiang riverine and estuarine hydromorphodynamic processes*. Springer Singapore.

Dai, Z. J., Fagherazzi, S., Gao, S., Mei, X. F., Ge, Z. P., & Wei, W. (2018b). Scaling properties of estuarine beaches. *Marine Geology*, *404*, 130–136. https://doi.org/10.1016/j.margeo.2018.07.011

Dai, Z. J., Liu, J. T., Fu, G., & Xie, H. L. (2013). A thirteen-year record of bathymetric changes in the north passage, Changjiang (Yangtze) estuary. *Geomorphology*, *187*, 101–107. https://doi.org/10.1016/j.geomorph.2013.01.004

Dai, Z. J., Liu, J. T., Wei, W., & Chen, J. Y. (2014). Detection of the Three Gorges Dam influence on the Changjiang (Yangtze River) submerged delta. *Scientific Reports*, *4*, 1–7.

Dai, Z. J., Liu, J. T., & Wen, W. (2015). Morphological evolution of the south passage in the Changjiang (Yangtze River) estuary, China. *Quaternary International*, *380*, 314–326. https://doi.org/10.1016/j.quaint.2015.01.045

Dai, Z. J., Mei, X. F., Darby, S. E., Lou, Y. Y., & Li, W. H. (2018a). Fluvial sediment transfer in the Changjiang (Yangtze) river-estuary depositional system. *Journal of Hydrology*, *566*, 719–734. https://doi.org/10.1016/j.jhydrol.2018.09.019

Deltares. (2014). User manual Delft3D-Flow: Simulation of multi-dimensional hydrodynamic flows and transport phenomena, including sediments. *Version 3.15, Delft, Netherlands*.

Dunn, F. E., Darby, S. E., Nicholls, R. J., Cohen, S., Zarfl, C., & Fekete, B. M. (2019). Projections of declining fluvial sediment delivery to major deltas worldwide in response to climate change and anthropogenic stress. *Environmental Research Letters*, *14*(8), 084034. https://doi.org/10.1088/1748-9326/ab304e

Edmonds, D. A., Toby, S. C., Siverd, C. G., Twilley, R., Bentley, S. J., Hagen, S., & Xu, K. H. (2023). Land loss due to human-altered sediment budget in the Mississippi River Delta. *Nature Sustainability*, *6*, 644–651. https://doi.org/10.1038/s41893-023-01081-0

Elmilady, H., van der Wegen, M., Roelvink, D., & Jaffe, B. E. (2019). Intertidal area disappears under sea level rise: 250 years of morphodynamic modeling in San Pablo Bay, California. *Journal of Geophysical Research: Earth Surface*, *124*(1), 38–59. https://doi.org/10.1029/2018JF004857

Elmilady, H., van der Wegen, M., Roelvink, D., & van der Spek, A. (2022). Modeling the morphodynamic response of estuarine intertidal shoals to sea-level rise. *Journal of Geophysical Research: Earth Surface*, *127*(1), e2021JF006152. https://doi.org/10.1029/2021JF006152

Erban, L. E., Gorelick, S. M., & Zebker, H. A. (2014). Groundwater extraction, land subsidence, and sea-level rise in the Mekong Delta, Vietnam. *Environmental Research Letters*, *9*(8), 084010. https://doi.org/10.1088/1748-9326/9/8/084010

Ericson, J. P., Vörösmarty, C. J., Dingman, S. L., Ward, L. G., & Meybeck, M. (2006). Effective sea-level rise and deltas: Causes of change and human dimension implications. *Global and Planetary Change*, *50*(1-2), 63–82. https://doi.org/10.1016/j.gloplacha.2005.07.004

Eslami, S., Hoekstra, P., Nguyen Trung, N., Ahmed Kantoush, S., Van Binh, D., Duc Dung, D., Quang, T. T., & van der Vegt, M. (2019). Tidal amplification and salt intrusion in the Mekong Delta driven by anthropogenic sediment starvation. *Scientific Reports*, *9*(1), 18746. https://doi.org/10.1038/s41598-019-55018-9

Fagherazzi, S., Edmonds, D. A., Nardin, W., Leonardi, N., Canestrelli, A., Falcini, F., Jerolmack, D. J., Mariotti, G., Rowland, J. C., & Slingerland, R. L. (2015). Dynamics of river mouth deposits. *Reviews of Geophysics*, *53*(3), 642–672. https://doi.org/10.1002/2014RG000451

Fagherazzi, S., Mariotti, G., Leonardi, N., Canestrelli, A., Nardin, W., & Kearney, W. S. (2020). Salt marsh dynamics in a period of accelerated sea level rise. *Journal of Geophysical Research: Earth Surface*, *125*(8), e2019JF005200. https://doi.org/10.1029/2019JF005200

Finotello, A., Lentsch, N., & Paola, C. (2019). Experimental delta evolution in tidal environments: Morphologic response to relative sea-level rise and net deposition. *Earth Surface Processes and Landforms*, *44*(10), 2000–2015. https://doi.org/10.1002/esp.4627

Gao, J. H., Shi, Y., Sheng, H., Kettner, A. J., Yang, Y., Jia, J. J., Wang, Y. P., Li, J., Chen, Y. N., Zou, X. Q., & Gao, S. (2019). Rapid response of the Changjiang (Yangtze) River and East China Sea source-to-sink conveying system to human induced catchment perturbations. *Marine Geology*, *414*, 1–17. https://doi.org/10.1016/j.margeo.2019.05.003

Goodbred, Jr. S. L., & Kuehl, S. A. (1999). Holocene and modern sediment budgets for the Ganges-Brahmaputra river system: Evidence for highstand dispersal to flood-plain, shelf, and deep-sea depocenters. *Geology*, *27*(6), 559–562. https://doi.org/10.1130/0091-7613(1999)027 < 0559:HAMSBF > 2.3.CO;2

GoodbredJrS. L., Kuehl, S. A., Steckler, M. S., & Sarker, M. H. (2003). Controls on facies distribution and stratigraphic preservation in the Ganges-Brahmaputra delta sequence. *Sedimentary Geology*, *155*(3-4), 301–316. https://doi.org/10.1016/S0037-0738(02)00184-7

Guo, X. J., Fan, D. D., Zheng, S., Wang, H. M., Zhao, B. C., & Qin, C. J. (2021). Revisited sediment budget with latest bathymetric data in the highly altered Yangtze (Changjiang) Estuary. *Geomorphology*, *391*, 107873. https://doi.org/10.1016/j.geomorph.2021.107873

Haney, R. L. (1991). On the pressure gradient force over steep topography in sigma coordinate ocean models. *Journal of Physical Oceanography*, *21*, 610–619. https://doi.org/10.1175/1520-0485(1991)021 < 0610:OTPGFO > 2.0.CO;2

He, Z. G., Tang, Y. L., Xia, Y. Z., Chen, B. D., Xu, J., Yu, Z. Z., & Li, L. (2020). Interaction impacts of tides, waves and winds on storm surge in a channel-island system: Observational and numerical study in Yangshan Harbor. *Ocean Dynamics*, *70*, 307–325. https://doi.org/10.1007/s10236-019-01328-5

Hoitink, A. J. F., Wang, Z. B., Vermeulen, B., Huismans, Y., & Kästner, K. (2017). Tidal controls on river delta morphology. *Nature Geoscience*, *10*(9), 637–645. https://doi.org/10.1038/ngeo3000

Hori, K., Saito, Y., Zhao, Q., Cheng, X. R., Wang, P. X., Sato, Y., & Li, C. X. (2001). Sedimentary facies and holocene progradation rates of the Changjiang (Yangtze) delta, China. *Geomorphology*, *41*(2-3), 233–248. https://doi.org/10.1016/S0169-555X(01)00119-2

Hori, K., Saito, Y., Zhao, Q., & Wang, P. X. (2002). Architecture and evolution of the tide-dominated Changjiang (Yangtze) River delta, China. *Sedimentary Geology*, *146*(3-4), 249–264. https://doi.org/10.1016/S0037-0738(01)00122-1

Ibàñez, C., Canicio, A., Day, J. W., & Curcó, A. (1997). Morphologic development, relative sea level rise and sustainable management of water and sediment in the Ebre Delta, Spain. *Journal of Coastal Conservation*, *3*, 191–202. https://doi.org/10.1007/BF02905244

Iwantoro, A. P., van der Vegt, M., & Kleinhans, M. G. (2022). Stability and asymmetry of tide-influenced river bifurcations. *Journal of Geophysical Research: Earth Surface*, *127*(6), e2021JF006282. https://doi.org/10.1029/2021JF006282

Jiang, C. J., Li, J. F., & de Swart, H. E. (2012). Effects of navigational works on morphological changes in the bar area of the Yangtze Estuary. *Geomorphology*, *139*, 205–219. https://doi.org/10.1016/j.geomorph.2011.10.020

Jiang, L., Gerkema, T., Idier, D., Slangen, A., & Soetaert, K. (2020). Effects of sea-level rise on tides and sediment dynamics in a Dutch tidal bay. *Ocean Science*, *16*(2), 307–321. https://doi.org/10.5194/os-16-307-2020

Khan, M. J. U., Durand, F., Testut, L., Krien, Y., & Islam, A. S. (2020). Sea level rise inducing tidal modulation along the coasts of Bengal delta. *Continental Shelf Research*, *211*, 104289. https://doi.org/10.1016/j.csr.2020.104289

Kuang, C. P., Chen, W., Gu, J., Zhu, D. Z., He, L. L., & Huang, H. C. (2014). Numerical assessment of the impacts of potential future sea-level rise on hydrodynamics of the Yangtze River Estuary, China. *Journal of Coastal Research*, *30*(3), 586–597. https://doi.org/10.2112/JCOASTRES-D-13-00149.1

Kuehl, S. A., DeMaster, D. J., & Nittrouer, C. A. (1986). Nature of sediment accumulation on the Amazon continental shelf. *Continental Shelf Research*, *6*(1-2), 209–225. https://doi.org/10.1016/0278-4343(86)90061-0

Leonardi, N., Mei, X. F., Carnacina, I., & Dai, Z. J. (2021). Marine sediment sustains the accretion of a mixed fluvial-tidal delta. *Marine Geology*, *438*, 106520. https://doi.org/10.1016/j.margeo.2021.106520

Li, J. F. (1991). The rule of sediment transport on the Nanhui tidal flat in the Changjiang Estuary. *Acta Oceanologica Sinica*, *1*, 117–127.

Li, J. F., Dai, Z. J., Liu, X. C., Zhao, J. C., & Feng, L. X. (2010). Research on the movement of water and suspended sediment and sedimentation in Nanhui spit of the Yangtze Estuary before and after the construction of the reclamation projects on the tidal flat. *Journal of Sediment Research*, *3*, 31–37. (in Chinese with English Abstract).

Li, J. F., Shi, W. R., & Shen, H. T. (1994). Sediment properties and transportation in the turbidity maximum in Changjiang Estuary. *Geographical Research*, *13*, 51–59.

Li, X., Liu, J. P., & Tian, B. (2016). Evolution of the jiuduansha wetland and the impact of navigation works in the Yangtze Estuary, China. *Geomorphology*, *253*, 328–339. https://doi.org/10.1016/j.geomorph.2015.10.031

Liu, J. P., Xu, K. H., Li, A. E. A., Milliman, J. D., Velozzi, D. M., Xiao, S. B., & Yang, Z. S. (2007). Flux and fate of Yangtze River sediment delivered to the East China Sea. *Geomorphology*, *85*(3-4), 208–224. https://doi.org/10.1016/j.geomorph.2006.03.023

Louters, T., van den Berg, J. H., & Mulder, J. P. (1998). Geomorphological changes of the Oosterschelde tidal system during and after the implementation of the delta project. *Journal of Coastal Research*, 1134–1151.

Luan, H. L., Ding, P. X., Wang, Z. B., & Ge, J. Z. (2017). Process-based morphodynamic modeling of the Yangtze Estuary at a decadal timescale: Controls on estuarine evolution and future trends. *Geomorphology*, *290*, 347–364. https://doi.org/10.1016/j.geomorph.2017.04.016

Luan, H. L., Ding, P. X., Yang, S. L., & Wang, Z. B. (2021). Accretion-erosion conversion in the subaqueous Yangtze Delta in response to fluvial sediment decline. *Geomorphology*, *382*, 107680. https://doi.org/10.1016/j.geomorph.2021.107680

Luo, J. J., Dai, Z. J., Wang, J., Lou, Y. Y., Zhou, X. Y., & Tang, R. N. (2023). Effects of human-induced riverine sediment transfer on deposition-erosion in the South Passage of the Changjiang (Yangtze) delta. *Journal of Hydrology*, *622*, 129714. https://doi.org/10.1016/j.jhydrol.2023.129714

Luo, X. X., Yang, S. L., & Zhang, J. (2012). The impact of the Three Gorges Dam on the downstream distribution and texture of sediments along the middle and lower Yangtze River (Changjiang) and its estuary, and subsequent sediment dispersal in the East China Sea. *Geomorphology*, *179*, 126–140. https://doi.org/10.1016/j.geomorph.2012.05.034

Mei, X. F., Dai, Z. J., Darby, S. E., Zhang, M., Cai, H. Y., Wang, J., & Wei, W. (2021). Landward shifts of the maximum accretion zone in the tidal reach of the Changjiang estuary following construction of the Three Gorges Dam. *Journal of Hydrology*, *592*, 125789. https://doi.org/10.1016/j.jhydrol.2020.125789

Mei, X. F., Dai, Z. J., Wei, W., Li, W. H., Wang, J., & Sheng, H. (2018). Secular bathymetric variations of the North Channel in the Changjiang (Yangtze) Estuary, People's Republic of China, 1880-2013: Causes and effects. *Geomorphology*, *303*, 30–40. https://doi.org/10.1016/j.geomorph.2017.11.014

Mei, X. F., Leonardi, N., Dai, J. X., & Wang, J. (2023). Cellular automata to understand the prograding limit of deltaic tidal flat. *Engineering Applications of Computational Fluid Mechanics*, *17*(1), 2234038. https://doi.org/10.1080/19942060.2023.2234038

Nhuan, M. T., & Van Ngoi, C. (2012). An analysis of coastal erosion in the tropical rapid accretion delta of the red river, Vietnam. *Journal of Asian Earth Sciences*, *43*(1), 98–109. https://doi.org/10.1016/j.jseaes.2011.08.014

Nicholls, R. J., Lincke, D., Hinkel, J., Brown, S., Vafeidis, A. T., Meyssignac, B., Hanson, S. E., Merkens, J., & Fang, J. Y. (2021). A global analysis of subsidence, relative sea-level change and coastal flood exposure. *Nature Climate Change*, *11*(4), 338–342. https://doi.org/10.1038/s41558-021-00993-z

Nienhuis, J. H., Ashton, A. D., Edmonds, D. A., Hoitink, A. J. F., Kettner, A. J., Rowland, J. C., & Törnqvist, T. E. (2020). Global-scale human impact on delta morphology has led to net land area gain. *Nature*, *577*, 514–518.

Nienhuis, J. H., Hoitink, A. J. F., & Törnqvist, T. E. (2018). Future change to tide-influenced deltas. *Geophysical Research Letters*, *45*(8), 3499–3507. https://doi.org/10.1029/2018GL077638

Nienhuis, J. H., Kim, W., Milne, G. A., Quock, M., Slangen, A. B., & Törnqvist, T. E. (2023). River deltas and sea-level rise. *Annual Review of Earth and Planetary Sciences*, *51*, 79–104. https://doi.org/10.1146/annurev-earth-031621-093732

Nienhuis, J. H., & van de Wal, R. S. (2021). Projections of global delta land loss from sea-level rise in the 21st century. *Geophysical Research Letters*, *48*(14), e2021GL093368. https://doi.org/10.1029/2021GL093368

Passeri, D. L., Hagen, S. C., Medeiros, S. C., Bilskie, M. V., Alizad, K., & Wang, D. (2015). The dynamic effects of sea level rise on low-gradient coastal landscapes: A review. *Earth's Future*, *3*(6), 159–181. https://doi.org/10.1002/2015EF000298

Passeri, D. L., Hagen, S. C., Plant, N. G., Bilskie, M. V., Medeiros, S. C., & Alizad, K. (2016). Tidal hydrodynamics under future sea level rise and coastal morphology in the Northern Gulf of Mexico. *Earth's Future*, *4*(5), 159–176. https://doi.org/10.1002/2015EF000332

Porebski, S. J., & Steel, R. J. (2006). Deltas and sea-level change. *Journal of Sedimentary Research*, *76*(3), 390–403. https://doi.org/10.2110/jsr.2006.034

Raff, J. L., Goodbred, Jr, S. L., Pickering, J. L., Sincavage, R. S., Ayers, J. C., Hossain, M. S., Wilson, C. A., Paola, C., Steckler, M. S., Mondal, D. R., Grimaud, J., Grall, C. J., Rogers, K. G., Ahmed, K. M., Akhter, S. H., Carlson, B. N., Chamberlain, E. L., Dejter, M., Gilligan, J. M., … Williams, L. A. (2023). Sediment delivery to sustain the Ganges-Brahmaputra delta under climate change and anthropogenic impacts. *Nature Communications*, *14*(1), 2429. https://doi.org/10.1038/s41467-023-38057-9

Sabatier, F., Samat, O., Ullmann, A., & Suanez, S. (2009). Connecting large-scale coastal behaviour with coastal management of the Rhone delta. *Geomorphology*, *107*(1-2), 79–89. https://doi.org/10.1016/j.geomorph.2006.09.026

Saintilan, N., Kovalenko, K. E., Guntenspergen, G., Rogers, K., Lynch, J. C., Cahoon, D. R., Lovelock, C. E., Friess, D. A., Ashe, E., Krauss, K. W., Cormier, N., Spencer, T., Adams, J., Raw, J., Ibanez, C., Scarton, F., Temmerman, S., Meire, P., Maris, T., … Khan, N. (2022). Constraints on the adjustment of tidal marshes to accelerating sea level rise. *Science*, *377*(6605), 523–527. https://doi.org/10.1126/science.abo7872

Schmitt, R. J., Giuliani, M., Bizzi, S., Kondolf, G. M., Daily, G. C., & Castelletti, A. (2021). Strategic basin and delta planning increases the resilience of the Mekong Delta under future uncertainty. *Proceedings of the National Academy of Sciences*, *118*(36), e2026127118. https://doi.org/10.1073/pnas.2026127118

Shaw, J. B., & Mohrig, D. (2014). The importance of erosion in distributary channel network growth, Wax Lake Delta, Louisiana, USA. *Geology*, *42*(1), 31–34. https://doi.org/10.1130/G34751.1

Shaw, J. B., Mohrig, D., & Whitman, S. K. (2013). The morphology and evolution of channels on the Wax Lake Delta, Louisiana, USA. *Journal of Geophysical Research: Earth Surface*, *118*(3), 1562–1584. https://doi.org/10.1002/jgrf.20123

Shen, H. T., He, S. L., Pan, D. G., & Li, J. F. (1992). A study of turbidity maximum in the Changjiang Estuary. *Acta Geographical Sinica*, *47*, 472–479.

Shen, H. T., & Li, J. F. (2011). *Water and sediment transport in Yangtze Estuary*. China Ocean Press.

Sibson, R. (1981). A brief description of natural neighbor interpolation. *Interpreting Multivariate Data*, 21–36, John Wiley & Sons, New York.

Syvitski, J., Ángel, J. R., Saito, Y., Overeem, I., Vörösmarty, C. J., Wang, H. J., & Olago, D. (2022). Earth's sediment cycle during the Anthropocene. *Nature Reviews Earth & Environment*, *3*(3), 179–196. https://doi.org/10.1038/s43017-021-00253-w

Syvitski, J. P., Kettner, A. J., Overeem, I., Hutton, E. W., Hannon, M. T., Brakenridge, G. R., Day, J., Vörösmarty, C., Saito, Y., Giosan, L., & Nicholls, R. J. (2009). Sinking deltas due to human activities. *Nature Geoscience*, *2*(10), 681–686. https://doi.org/10.1038/ngeo629

Szczuciński, W., Jagodziński, R., Hanebuth, T. J., Stattegger, K., Wetzel, A., Mitręga, M., Unverricht, D., & Van Phach, P. (2013). Modern sedimentation and sediment dispersal pattern on the continental shelf off the Mekong river delta, South China Sea. *Global and Planetary Change*, *110*, 195–213. https://doi.org/10.1016/j.gloplacha.2013.08.019

Talke, S. A., & Jay, D. A. (2020). Changing tides: The role of natural and anthropogenic factors. *Annual Review of Marine Science*, *12*, 121–151. https://doi.org/10.1146/annurev-marine-010419-010727

Tang, Z. H. (2008). Evaluating local coastal zone land use planning capacities in California. *Ocean & Coastal Management*, *51*(7), 544–555. https://doi.org/10.1016/j.ocecoaman.2008.06.001

Tang, Z. H., Dai, Z. J., Fu, X. Y., & Li, X. (2013). Content analysis for the US coastal states' climate action plans in managing the risks of extreme climate events and disasters. *Ocean & Coastal Management*, *80*, 46–54. https://doi.org/10.1016/j.ocecoaman.2013.04.004

Tessler, Z. D., Vörösmarty, C. J., Grossberg, M., Gladkova, I., Aizenman, H., Syvitski, J. P., & Foufoula-Georgiou, E. (2015). Profiling risk and sustainability in coastal deltas of the world. *Science*, *349*(6248), 638–643. https://doi.org/10.1126/science.aab3574

Tessler, Z. D., Vörösmarty, C. J., Overeem, I., & Syvitski, J. P. (2018). A model of water and sediment balance as determinants of relative sea level rise in contemporary and future deltas. *Geomorphology*, *305*, 209–220. https://doi.org/10.1016/j.geomorph.2017.09.040

Thanh, V. Q., Reyns, J., Van, S. P., Anh, D. T., Dang, T. D., & Roelvink, D. (2019). Sediment transport and morphodynamical modeling on the estuaries and coastal zone of the Vietnamese Mekong Delta. *Continental Shelf*

Research, *186*, 64–76. https://doi.org/10.1016/j.csr.2019.07.015

van Binh, D., Kantoush, S., & Sumi, T. (2020). Changes to long-term discharge and sediment loads in the Vietnamese Mekong Delta caused by upstream dams. *Geomorphology*, *353*, 107011. https://doi.org/10.1016/j.geomorph.2019.107011

van De Lageweg, W. I., & Slangen, A. B. (2017). Predicting dynamic coastal delta change in response to sea-level rise. *Journal of Marine Science and Engineering*, *5*(2), 24. https://doi.org/10.3390/jmse5020024

van der Spek, A. J., & Elias, E. P. (2021). Half a century of morphological change in the Haringvliet and Grevelingen ebb-tidal deltas (SW Netherlands)-impacts of large-scale engineering 1964-2015. *Marine Geology*, *432*, 106404. https://doi.org/10.1016/j.margeo.2020.106404

van der Wegen, M. (2013). Numerical modeling of the impact of sea level rise on tidal basin morphodynamics. *Journal of Geophysical Research: Earth Surface*, *118*(2), 447–460. https://doi.org/10.1002/jgrf.20034

van der Wegen, M., Jaffe, B., Foxgrover, A., & Roelvink, D. (2017). Mudflat morphodynamics and the impact of sea level rise in South San Francisco Bay. *Estuaries and Coasts*, *40*(1), 37–49. https://doi.org/10.1007/s12237-016-0129-6

van der Wegen, M., & Jaffe, B. E. (2014). Processes governing decadal-scale depositional narrowing of the major tidal channel in San Pablo Bay, California, USA. *Journal of Geophysical Research: Earth Surface*, *119*(5), 1136–1154. https://doi.org/10.1002/2013JF002824

van Maanen, B., Coco, G., Bryan, K. R., & Friedrichs, C. T. (2013). Modeling the morphodynamic response of tidal embayments to sea-level rise. *Ocean Dynamics*, *63*, 1249–1262. https://doi.org/10.1007/s10236-013-0649-6

Vasilopoulos, G., Quan, Q. L., Parsons, D. R., Darby, S. E., Tri, V. P. D., Hung, N. N., Haigh, I. D., Voepel, H. E., Nicholas, A. P., & Aalto, R. (2021). Establishing sustainable sediment budgets is critical for climate-resilient mega-deltas. *Environmental Research Letters*, *16*, 064089.

Vellinga, N. E., Hoitink, A. J. F., van der Vegt, M., Zhang, W., & Hoekstra, P. (2014). Human impacts on tides overwhelm the effect of sea level rise on extreme water levels in the Rhine-Meuse delta. *Coastal Engineering*, *90*, 40–50. https://doi.org/10.1016/j.coastaleng.2014.04.005

Vinh, V. D., Ouillon, S., Thanh, T. D., & Chu, L. V. (2014). Impact of the Hoa Binh dam (Vietnam) on water and sediment budgets in the Red River basin and delta. *Hydrology and Earth System Sciences*, *18*(10), 3987–4005. https://doi.org/10.5194/hess-18-3987-2014

Wang, J., Dai, Z. J., Fagherazzi, S., Lou, Y. Y., Mei, X. F., & Ma, B. B. (2023). Large-scale sedimentary shift induced by a mega dam in deltaic flats. *Sedimentology*, https://doi.org/10.1111/sed.13168

Wang, J., Dai, Z. J., Fagherazzi, S., Zhang, X. H., & Liu, X. Q. (2022a). Hydro-morphodynamics triggered by extreme riverine floods in a mega fluvial-tidal delta. *Science of The Total Environment*, *809*, 152076. https://doi.org/10.1016/j.scitotenv.2021.152076

Wang, J., Dai, Z. J., Mei, X. F., & Fagherazzi, S. (2020). Tropical cyclones significantly alleviate mega-deltaic erosion induced by high riverine flow. *Geophysical Research Letters*, *47*, e2020GL089065.

Wang, J., Dai, Z. J., Wei, W., Ge, Z. P., Pang, W. H., Ma, B. B., Mei, X. F., & Yu, Y. W. (2018a). LiDAR-based recent morphodynamic study of south Nanhui tidal flat, Changjiang Estuary. *Oceanologia et Limnologia Sinica*, *49*, 756–768. (in Chinese with English Abstract).

Wang, Y. H., Dong, P., Oguchi, T., Chen, S. L., & Shen, H. T. (2013). Long-term (1842-2006) morphological change and equilibrium state of the Changjiang (Yangtze) Estuary, China. *Continental Shelf Research*, *56*, 71–81. https://doi.org/10.1016/j.csr.2013.02.006

Wang, Z. H., Saito, Y., Zhan, Q., Nian, X. M., Pan, D. D., Wang, L., Chen, T., Xie, J. L., Li, X., & Jiang, X. Z. (2018b). Three-dimensional evolution of the Yangtze River mouth, China during the Holocene: Impacts of sea level, climate and human activity. *Earth-Science Reviews*, *185*, 938–955. https://doi.org/10.1016/j.earscirev.2018.08.012

Wei, W., Dai, Z. J., Mei, X. F., Liu, J. P., Gao, S., & Li, S. S. (2017). Shoal morphodynamics of the Changjiang (Yangtze) estuary: Influences from river damming, estuarine hydraulic engineering and reclamation projects. *Marine Geology*, *386*, 32–43. https://doi.org/10.1016/j.margeo.2017.02.013

Wei, W., Dai, Z. J., Pang, W. H., Wang, J., & Gao, S. (2020). Sedimentary zonation shift of tidal flats in a meso-tidal estuary. *Sedimentary Geology*, *407*, 105749. https://doi.org/10.1016/j.sedgeo.2020.105749

Wei, W., Mei, X. F., Dai, Z. J., & Tang, Z. H. (2016). Recent morphodynamic evolution of the largest uninhibited island in the Yangtze (Changjiang) estuary during 1998–2014: Influence of the anthropogenic interference. *Continental Shelf Research*, *124*, 83–94. https://doi.org/10.1016/j.csr.2016.05.011

Woodroffe, C. D., & Murray-Wallace, C. V. (2012). Sea-level rise and coastal change: The past as a guide to the future. *Quaternary Science Reviews*, *54*, 4–11. https://doi.org/10.1016/j.quascirev.2012.05.009

Wu, Z. Y., Milliman, J. D., Zhao, D. N., Zhou, J. Q., & Yao, C. H. (2014). Recent geomorphic change in LingDing Bay, China, in response to economic and urban growth on the Pearl River Delta, Southern China. *Global and Planetary Change*, *123*, 1–12. https://doi.org/10.1016/j.gloplacha.2014.10.009

Xie, D. F., Pan, C. H., Wu, X. G., Gao, S., & Wang, Z. B. (2017). The variations of sediment transport patterns in the outer Changjiang Estuary and Hangzhou Bay over the last 30 years. *Journal of Geophysical Research: Oceans*, *122*(4), 2999–3020. https://doi.org/10.1002/2016JC012264

Xue, Z., Liu, J. P., DeMaster, D., Van Nguyen, L., & Ta, T. K. O. (2010). Late Holocene evolution of the Mekong subaqueous delta, southern Vietnam. *Marine Geology*, *269*(1-2), 46–60. https://doi.org/10.1016/j.margeo.2009.12.005

Yang, S. L., Xu, K. H., Milliman, J. D., Yang, H. F., & Wu, C. S. (2015). Decline of Yangtze River water and sediment discharge: Impact from natural and anthropogenic changes. *Scientific Reports*, *5*(1), 12581. https://doi.org/10.1038/srep12581

Yang, S. L., Zhang, J., Zhu, J., Smith, J. P., Dai, S. B., Gao, A., & Li, P. (2005). Impact of dams on Yangtze River sediment supply to the sea and delta intertidal wetland response. *Journal of Geophysical Research: Earth Surface*, *110*, F03006.

Yin, Y., Karunarathna, H., & Reeve, D. E. (2019). Numerical modelling of hydrodynamic and morphodynamic response of a meso-tidal estuary inlet to the impacts of

global climate variabilities. *Marine Geology*, *407*, 229–247. https://doi.org/10.1016/j.margeo.2018.11.005

Yun, C. X. (2004). *Basic law of the recent evolution of the Changjiang Estuary*. People's Republic of China Ocean Press. (in Chinese).

Zhan, Q., Li, M. T., Liu, X. Q., Chen, J., & Chen, Z. Y. (2020). Sedimentary transition of the Yangtze subaqueous delta during the past century: Inspiration for delta response to future decline of sediment supply. *Marine Geology*, *428*, 106279. https://doi.org/10.1016/j.margeo.2020.106279

Zhang, X. D., Zhang, Y. X., Zhu, L. H., Chi, W. Q., Yang, Z. S., Wang, B. Y., Lv, K., Wang, H. M., & Lu, Z. Y. (2018b). Spatial-temporal evolution of the eastern Nanhui mudflat in the Changjiang (Yangtze River) Estuary under intensified human activities. *Geomorphology*, *309*, 38–50. https://doi.org/10.1016/j.geomorph.2018.02.023

Zhang, X. H., Fagherazzi, S., Leonardi, N., & Li, J. F. (2018a). A positive feedback between sediment deposition and tidal prism may affect the morphodynamic evolution of tidal deltas. *Journal of Geophysical Research: Earth Surface*, *123*(11), 2767–2783. https://doi.org/10.1029/2018JF004639

Zhao, L. H., Xin, P., Cheng, H. F., & Chu, A. (2023). Change of turbidity maximum in Yangtze estuary after construction of the Three Gorges Dam. *Continental Shelf Research*, *258*, 104983. https://doi.org/10.1016/j.csr.2023.104983

Zhu, B. Y., Yue, Y., Borthwick, A. G., Yu, W. J., Liang, E. H., Tang, J. W., Chai, Y. F., & Li, Y. T. (2020). Decadal link between longitudinal morphological changes in branching channels of Yangtze estuary and movement of the offshore depo-center. *Earth Surface Processes and Landforms*, *45*(11), 2689–2705. https://doi.org/10.1002/esp.4923

Zhu, L., He, Q., Shen, J., & Wang, Y. Y. (2016). The influence of human activities on morphodynamics and alteration of sediment source and sink in the Changjiang Estuary. *Geomorphology*, *273*, 52–62. https://doi.org/10.1016/j.geomorph.2016.07.025

Zou, X. Q., & Gao, S. (2019). Rapid response of the Changjiang (Yangtze) River and East China Sea source-to-sink conveying system to human induced catchment perturbations. *Marine Geology*, *414*, 1–17. https://doi.org/10.1016/j.margeo.2019.05.003